



HAL
open science

An experimental and kinetic investigation of premixed furan/oxygen/argon flames

Z. Tian, T. Yuan, R. Fournet, P.A. Glaude, B. Sirjean, F. Battin-Leclerc, K. Zhang, F. Qi

► **To cite this version:**

Z. Tian, T. Yuan, R. Fournet, P.A. Glaude, B. Sirjean, et al.. An experimental and kinetic investigation of premixed furan/oxygen/argon flames. *Combustion and Flame*, 2011, 158, pp.756-773. 10.1016/j.combustflame.2010.12.022 . hal-00576339

HAL Id: hal-00576339

<https://hal.science/hal-00576339>

Submitted on 14 Mar 2011

HAL is a multi-disciplinary open access archive for the deposit and dissemination of scientific research documents, whether they are published or not. The documents may come from teaching and research institutions in France or abroad, or from public or private research centers.

L'archive ouverte pluridisciplinaire **HAL**, est destinée au dépôt et à la diffusion de documents scientifiques de niveau recherche, publiés ou non, émanant des établissements d'enseignement et de recherche français ou étrangers, des laboratoires publics ou privés.

An experimental and kinetic investigation of premixed furan/oxygen/argon flames

Zhenyu Tian ^{1,2,†}, Tao Yuan ², Rene Fournet ¹, Pierre-Alexandre Glaude ¹, Baptiste Sirjean ¹,
Frédérique Battin-Leclerc ^{1,*}, Kuiwen Zhang ², Fei Qi ^{2,*}

¹ Laboratoire Réactions et Génie des Procédés, CNRS, Nancy Université, ENSIC, 1, rue Grandville, BP 451, 54001
Nancy Cedex, France

² National Synchrotron Radiation Laboratory, University of Science and Technology of China,
Hefei, Anhui 230029, P. R. China

TITLE RUNNING HEAD: Experimental and modeling study of premixed furan flames.

Corresponding authors

Dr. Frédérique Battin-Leclerc (FBL)

Email: Frederique.Battin-Leclerc@ensic.inpl-nancy.fr

Tel: 0033(0)3 83 17 51 25

Fax: 0033(0)3 83 37 81 20

Prof. Fei Qi (FQ)

Email: fqi@ustc.edu.cn

Tel: 0086(0)551 3602125

Fax: 0086(0)551 5141078

[†] Current address: Physikalische Chemie I, Universität Bielefeld, Universitätsstr. 25, 33615 Bielefeld, Germany.

^{*} Corresponding authors. E-mail address: Frederique.Battin-Leclerc@ensic.inpl-nancy.fr, fqi@ustc.edu.cn.

ABSTRACT: The detailed chemical structures of three low-pressure (35 Torr) premixed laminar furan/oxygen/argon flames with equivalence ratios of 1.4, 1.8 and 2.2 have been investigated by using tunable synchrotron vacuum ultraviolet (VUV) photoionization and molecular-beam mass spectrometry. About 40 combustion species including hydrocarbons and oxygenated intermediates have been identified by measurements of photoionization efficiency spectra. Mole fraction profiles of the flame species including reactants, intermediates and products have been determined by scanning burner position with some selected photon energies near ionization thresholds. Flame temperatures have been measured by a Pt-6%Rh/Pt-30%Rh thermocouple. A new mechanism involving 206 species and 1368 reactions has been proposed whose predictions are in reasonable agreement with measured species profiles for the three investigated flames. Rate-of-production and sensitivity analyses have been performed to track the key reaction paths governing furan consumption for different equivalence ratios. Both experimental and modeling results indicate that few aromatics could be formed in these flames. Furthermore, the current model has been validated against previous pyrolysis results of the literature obtained behind shock waves and the agreement is reasonable as well.

KEYWORDS: Premixed laminar flame; Kinetic modeling; Furan; Tunable synchrotron VUV photoionization; Molecular-beam mass spectrometry.

1. Introduction

The interest for studying the gas-phase reactions of biofuels, mainly alcohols, ethers and biodiesels, has increased in recent years because they offer the long-term promise of fuel-source regenerability and reduced climatic impact [1]. In engine tests, Avantium Company demonstrated that furan-based biofuels, or “furanics” were potential biofuels and had significant advantages over first-generation biofuels [2,3]. For example, 2,5-dimethylfuran (DMF) has an energy density 40% greater than ethanol, which is comparable to that of gasoline. Furan and its derivatives have also been identified among the emissions produced from the biomass burning and the combustion of fossil fuels [4-6]. Investigations with pyrolysis of leaf and wood indicate that furan is one of the major degradation products of these compounds [7]. In addition, furan has also been proved to be a significant component of tobacco smoke [8] and is selected as a model oxygenated reburn fuel for NO reduction [9]. Therefore, it is necessary to understand the combustion chemistry of furan.

Previous studies relevant to the gas phase reactions of furan were mainly focused on experiments and modeling of its thermal decomposition [10-18]. In 1972, Cullis and Norris [10] studied the pyrolysis of furan within the temperature range of 1173 – 1323 K at 1 atm. The main products observed were methane (CH₄), acetylene (C₂H₂), ethylene (C₂H₄), and benzene (C₆H₆). With a heated flow reactor and an on-line mass spectrometry (MS), Grela et al. [11] investigated the low-pressure (10⁻³ Torr, 760 Torr = 1 atm) pyrolysis of furan over the temperature range of 1050 – 1270 K and found the presence of C₃H₄ (allene, aC₃H₄/propyne, pC₃H₄) and CO. They also proposed a high-pressure Arrhenius expression $k_{\infty} = 10^{15.6} \exp(-73.5 \text{ kcal}\cdot\text{mol}^{-1}/RT) \text{ s}^{-1}$ as the rate constant for furan decomposition. Later, Bruinsma et al. [13] studied the decomposition of furan within the temperature range of 960 – 1085 K at 1 Torr. CO and C₃H₄ were identified and a very different Arrhenius equation, $k = 10^{12.9} \exp(-65.7 \text{ kcal}\cdot\text{mol}^{-1}/RT) \text{ s}^{-1}$, was reported. Three groups [12,14,15] carried out the thermal decomposition of furan behind shock waves. Lifshitz et al. [12] studied the decomposition of furan over the temperature range 1050 – 1460 K at gas densities of 3·10⁻⁵ mol/cm³ (2.6 – 3.6 atm) and proposed that the two main pathways of furan decomposition were due to CO +

pC₃H₄ and C₂H₂ + ketene (CH₂CO). By gas chromatography/mass spectrometry (GC/MS) analysis, they identified CO, pC₃H₄, C₂H₂ and indirectly, CH₂CO, as the major products and CH₄, aC₃H₄, C₂H₄, diacetylene (C₄H₂), vinylacetylene (C₄H₄), 1,3-butadiene (C₄H₆) and C₆H₆ as minor products [12]. Based on their measurements, they obtained the rate constant $k = 10^{15.43 \pm 0.45} \exp[-(78.3 \pm 2.0) \text{ kcal} \cdot \text{mol}^{-1} / \text{RT}] \text{ s}^{-1}$ for the overall decomposition of furan in the temperature range 1060 – 1260 K [12]. Organ and Mackie [14] extended the temperature range to 1100 – 1700 K (20 atm) and obtained the same conclusion as that of Lifshitz et al. [12] by detecting CO, pC₃H₄, C₂H₂ and CH₂CO directly. The global rate of furan decomposition was given as $k = 10^{15.3 \pm 0.3} \exp[-(77.9 \pm 1.9) \text{ kcal} \cdot \text{mol}^{-1} / \text{RT}] \text{ s}^{-1}$ and the initiation was postulated to be the homolytic C-O bond scission leading to a biradical [14]. With laser-schlieren (LS) and time-of-flight (TOF) MS detection techniques, Fulle et al. [15] confirmed the two dominant dissociation channels in the temperature range 1300 – 3000 K (600 Torr) and $k = 10^{15.3} \exp[-78.7 \text{ kcal} \cdot \text{mol}^{-1} / \text{RT}] \text{ s}^{-1}$ was given. Later, Winkler et al. [16] investigated the continuous flow pyrolysis of furan at 1173 K (1 atm) and up to 22 products were identified by GC-MS. They suggested that aromatics were generated from C₂- and C₃- species and found no tendency for the oxygen containing fragments of furan to form larger molecules. Recently, Hore et al. [17] studied the pyrolysis of furan using a combination of infrared laser powered homogeneous pyrolysis, chemical and physical trapping of radicals and precursors specifically designed to generate selected radicals in the temperature range 950 – 1000 K (~7 Torr) and confirmed the key role of 1,2-H shifts in the theoretical studies (see discussion below). More recently, Vasiliou et al. [18] performed furan decomposition with a high-temperature nozzle as a tubular reactor. They also demonstrated the importance of (CO + pC₃H₄) and (C₂H₂ + CH₂CO) routes; however, furan could also decompose to produce propargyl radical at a temperature higher than $1550 \pm 100 \text{ K}$ [18].

Despite the numerous experimental investigations of furan thermal decomposition, there were only three theoretical calculations concerning these reactions. Liu et al. [19,20] explored the thermal decomposition of furan with density functional (B3LYP) techniques for geometries and QCISD(T)

for energies. They reported the energetics of furan decomposition channels, but gave no information about rate constants. In 2000, Sendt et al. [21] obtained the thermochemistry and rate parameters of several key reactions related to furan at CASSCF, CASPT2 and G2-(MP2) levels. They proposed a detailed kinetic model and validated it against furan pyrolysis data measured by Organ and Mackie [14]; they concluded that the formation of cyclic intermediates and the formation of decomposition products ($\text{CO} + \text{pC}_3\text{H}_4$) initiated by 1,2-H transfer were the dominant pathways for furan pyrolysis. However, compared to such studies on the thermal decomposition of this molecule, no literature exists on its combustion.

In the present work, low-pressure premixed furan/ O_2 /Ar flames with three equivalence ratios (Φ) of 1.4 (flame A), 1.8 (flame B) and 2.2 (flame C) have been investigated with the molecular-beam mass spectrometry (MBMS) and tunable VUV synchrotron photoionization techniques [22-24]. Many flame species have been detected and identified by comparing the measured ionization energies (IE) with literature ones; their mole fraction profiles have been determined as well. Moreover, a detailed kinetic model has been developed based on the experimental measurements and reaction pathways were proposed with particular attention to the formation of the major intermediates.

2. Experimental Section

The experiments were performed at National Synchrotron Radiation Laboratory, Hefei, China. The instrument and data analysis procedures have been reported previously [25,26]. Briefly, the apparatus is composed of a flame chamber which contains a movable flat-flame burner (McKenna Burner) with 6 cm diameter, a differentially pumped chamber with a molecular-beam sampling system, and a photoionization chamber installed with a home-made reflectron time-of-flight mass spectrometer (RTOF-MS). Combustion species are sampled by a quartz cone with a 40° included angle and a ~ 500 μm orifice at the tip. The resulting molecular beam passes into a differentially pumped ionization region through a nickel skimmer, and then crosses with the tunable VUV

synchrotron light in the photoionization chamber. The photoions are collected and analyzed by the RTOF-MS with an approximate mass resolution of 1400 [22]. The integrated ion intensities for a specific mass are normalized by the photon flux, and then plotted as a function of the photon energy or distance from the burner surface, which then yields photoionization efficiency (PIE) or mole fraction profiles, respectively. Considering the cooling effect of molecular beam [27], the experimental error for determining IE is within 0.05 eV for stable species and slightly higher for some radicals because of the weak signal-to-noise ratio. The uncertainties of the mole fractions are ± 5 -10% for the major species, ± 25 % for intermediates with known photoionization cross sections and a factor of two for those with estimated cross sections.

Three flames from slightly rich ($\Phi = 1.4$, C/O = 0.538) to nearly sooting conditions ($\Phi = 2.2$, C/O = 0.786) were investigated. Flow rates of the gas reagents are controlled separately by MKS mass flow controllers, while the flow rates of liquid fuels into the vaporizer are controlled by a syringe pump (ISCO 1000D, USA). Furan was purchased from Sinopharm Chemical Reagent Limited Co., Shanghai, China with the purity of $\geq 99.5\%$. No further purification was carried out for this study. The operating conditions are listed in Table 1. For comparison, the pressure was kept at 35 Torr; the flow rate of Ar has a constant value of 1.000 standard liter per minute (SLM) and the cold-gas velocity is 33.49 cm/s for all flames. The temperature profiles have been measured by using a Pt-6%Rh/Pt-30%Rh thermocouple, 0.100 mm in diameter and 15 mm upstream from the sampling cone, with an Y_2O_3 -BeO anti-catalytic coating [27]. Radiation heat losses have been considered and calibrated for the temperature profiles [28], the detailed procedures of which were described in [29]. Based on the reproducibility of the measurement, the accuracy of the temperature measurements was estimated to be ± 100 K, within which the modeling results have a 3% uncertainty for the major species and about 10% for intermediates [29].

3. Kinetic model

To simulate the species profiles measured in the three furan flames, a new kinetic mechanism has been developed. Table 2 lists the reactions related to furan and derived species. This mechanism

was coupled with our recent mechanism which has been developed for the oxidation of toluene [30]. The complete mechanism (206 species and 1368 reactions) is available as supplementary material and only the primary and secondary reaction pathways are described here. Most thermochemical data have been estimated by the software THERGAS based on group additive method [31]. Some intermediate species derived from furan and those involving a missing group in the THERGAS software were estimated by ab initio calculation. The ab initio calculations were performed at the CBS-QB3 level [32] implemented in Gaussian 03 [33]. Enthalpies of formation at 298 K have been obtained from isodesmic reactions, while thermochemical properties as a function of temperature have been calculated using the CHEMRATE software [34] according to statistical mechanical principles. Hindered rotors have been taken into account and relaxed scans have been performed at the B3LYP/6-31G+(2d,p) level to determine the barrier of rotation. Table 3 presents the names, the formulae and the enthalpies of formation ($\Delta_f H^\circ$) of furan and its derived species which were not presented in our previous work [30].

3.1 Primary mechanism

The primary mechanism contains the reactions of furan and of the radicals directly derived from it. The unimolecular initiations of furan have been considered and Fig. 1 presents the simplified potential energy surface. According to Sendt et al.'s study [21], the most important unimolecular pathways for furan decomposition are the reactions involving 1,2-H migrations, which then lead to the formation of two different cyclic carbenes. These species can decompose to give the major products as CO + pC₃H₄ and C₂H₂ + CH₂CO. For the first route, Sendt et al. [21] showed that two rate-determining steps must be taken into account. The first one corresponds to the initial 1,2-H transfer from furan to form formyl allene (FA, $\text{CH}_2=\text{C}=\overset{\text{H}}{\text{C}}=\text{O}$, CH₂CCHCHO, 1,2-butadienal), (reaction 1 (R1) in Table 2), while the second step is related to the decomposition of FA by a concerted reaction (TS2) in which a 1,4-H transfer and a simultaneous C-C bond fission occurs to form CO and pC₃H₄ (R52). It must be noted that the decomposition of FA to propargyl and CHO radical (R51) has been also considered in our mechanism in accordance with the work of Sendt et al.


[21].

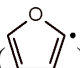

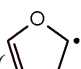

The detailed mechanism for the second unimolecular reaction of furan involves three elementary steps. The first one corresponds to the formation of a cyclic carbene (1,2-H shift) as discussed previously. The second step is related to the ring opening of the cyclic carbene to produce a diradical while the third step involved two successive bond cleavages of this latter species to form C_2H_2 and CH_2CO . It is possible, as mentioned by Sendt et al. [21], to calculate the overall rate constant by considering the last transition state TS3 which corresponds to the highest energy barrier involved in the overall reaction (Fig. 1).

All the calculations have been performed with the CBS-QB3 method [32] and the activation energies found are in a good agreement with those obtained by Sendt et al. [21] at the G2B2 and CASS-SCF level. Frequency analysis makes it possible to point out one imaginary frequency for each transition state (TS). High-pressure limit unimolecular rate constants were calculated using canonical transition state theory. The kinetic parameters were obtained with a modified Arrhenius form (Table 2).

An interesting feature, resulting from previous calculations, is the relatively low barriers involved in the unimolecular initiations. Consequently, these reactions become very important and their rate constants are sensitive parameters. Thus, we performed RRKM calculations in order to take into account pressure effect under flame conditions. Time dependent master equation has been solved with the CHEMRATE program [34] for the two pathways involved in Fig. 1. Calculations have been performed at 4.7 kPa and $T = 700-2000$ K. A ΔE_{down}^0 value of 260 cm^{-1} was used in the master equation analysis, with Ar as third body [35]. Lennard-Jones parameters for furan and other

isomers (FA) were estimated as $\sigma = 5.18 \text{ \AA}$ and $\frac{\epsilon}{k_b} = 357 \text{ K}$ in accordance with Joshi and Wang [35]. Rate constants, $k(E)$ have been estimated at 25 cm^{-1} ($0.07 \text{ kcal mol}^{-1}$) increments. The low-pressure rates (4.7 kPa) were used in the simulation of flame results, while the high pressure ones in pyrolysis conditions.

The kinetics of the unimolecular decompositions to give H atoms and furyl radicals (R3 and R4) have been deduced from those of the reverse reactions, $k = 1.0 \times 10^{14} \text{ s}^{-1}$ according to Allara and Shaw [36]. For the bimolecular initiations with oxygen molecules (R5 and R6), A-factors have been obtained using the correlation proposed by Ingham et al. [37] and the activation energies have been taken equal to the enthalpies of reaction. The rate constants of the additions of H and OH to furan (R7-R9) have been deduced from value proposed for the similar reactions in case of 1,3-butadiene [38] and our previous work on the oxidation of alkenes [39], respectively. The rate for the reaction of furan with CH_3 forming 2-methylfuran () and H (R10) has been taken from the reverse reaction proposed by Lifshitz et al. [40]. The kinetics for the abstractions of vinylic H atoms (R11-R18) were deduced from the correlations proposed by Heyberger et al. [39].

Two furyl radicals, furyl-2 () and furyl-3 () are formed by H-abstractions and two $\text{C}_4\text{H}_5\text{O}$ radicals, dihydrofuryl-2 (, $\text{C}_4\text{H}_5\text{O}-2$) and dihydrofuryl-3 (, $\text{C}_4\text{H}_5\text{O}-3$) are produced by H-additions. Isomerization reactions between the two furyl (R19) and the two $\text{C}_4\text{H}_5\text{O}$ radicals (R28) are possible. The rate constants of the isomerizations are deduced from the similar reaction of n- C_4H_5 and i- C_4H_5 radicals for furyl radicals [41], and from that of $\text{CH}_2=\text{CH}-\text{CH}_2-\text{CH}_2$ and $\text{CH}_2=\text{CH}-\text{CH}-\text{CH}_3$ radicals for $\text{C}_4\text{H}_5\text{O}$ radicals [38].

The decomposition reactions of furyl radicals have been also investigated at the CBS-QB3 level of theory [32]. Even if the bond dissociation energy of C-H is very high (about $119 \text{ kcal mol}^{-1}$ according to our calculations), the decomposition of these radicals could play a significant kinetic role under flame conditions where the high temperature and concentration of radicals favor H-abstractions from furan.

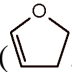

Figure 2 shows the major routes of decomposition of furyl radicals. All the activation energies shown in Figs. 2 and 3 have been calculated. For furyl-2, the β -scission of the C-O bond (R20) involves an activation energy of $33.7 \text{ kcal mol}^{-1}$, which is about 26 kcal mol^{-1} lower than the

corresponding C-C bond breaking. Thus, the last reaction was not considered in this study. The radical formed by ring opening can decompose either by C-H bond breaking, yielding ethynylketene ($\text{O}=\text{C}=\text{CH}-\text{C}\equiv\text{CH}$, $\text{C}_4\text{H}_2\text{O}$) (R39) or by β -scission of the C-C bond to form C_2H_2 and HCCO radical (R38). For furyl-3, only the β -scission of the C-O bond is possible with an activation energy of 31 kcal mol^{-1} (Fig. 2, R21). Three mesomeric forms exist for the radical obtained by ring opening but only one can decompose by C-H bond breaking to form $\text{C}_4\text{H}_2\text{O}$ (R41) or by isomerization followed by a β -scission yielding CO and propargyl radical (R40) with a very low activation energy (7.6 kcal mol^{-1}).


The high concentration of H atoms formed in flame can contribute to the formation of $\text{C}_4\text{H}_5\text{O}$ radicals by addition of H atoms on the double bond of furan. Figure 3 shows the principal routes of decomposition of $\text{C}_4\text{H}_5\text{O}$ radicals considered in our mechanism, which have been theoretically investigated. The $\text{C}_4\text{H}_5\text{O}$ -2 radical can react by C-C or C-O bond breaking to form a non-cyclic radical. The β -scission of C-O bond (R29) involves an activation energy of 35.3 kcal mol^{-1} against 43.9 kcal mol^{-1} for the C-C bond breaking while the β -scission of the linear radicals formed implies, in each case, a lower activation energy. Both routes lead to the formation of C_2H_2 and CH_2CHO radicals. Thus, only the C-O bond breaking has been considered here. The $\text{C}_4\text{H}_5\text{O}$ -3 radical can react by β -scission of the C-O bond (R30), with a low activation energy of 22 kcal mol^{-1} , forming a resonance stabilized radical. The latter can react by 1,5-H transfer (R44) followed by a decomposition to give C_2H_2 and CHCH_2OH (R46). A second pathway involved 1,2-H transfer (R45) followed by the subsequent β -scission to form CO and allyl radical. The two decomposition routes have been considered since in each case, an activation energy of about 47 kcal mol^{-1} is involved in the rate determining step.

In addition, the furyl radicals could react with oxygen (R22-R25) or O atoms (R26 and R27) with the kinetics estimated by analogy with similar reactions of C_2H_3 radicals [42,43]. Similarly, the $\text{C}_4\text{H}_5\text{O}$ radicals can be consumed by oxygen (R31 and R32) or O atoms (R33 and R34), the rate constants of which have been estimated by using the correlations proposed by Touchard et al. [44]

and by analogy with data by Baulch et al. [45], respectively.

Termination steps were written for CHCCHCHO ($\text{HC}=\overset{\text{O}\cdot}{\text{C}}-\text{CH}=\text{C}\equiv\text{CH}$), $\text{CH}_2\text{CHCHCHO}$ ($\text{HC}=\overset{\text{O}\cdot}{\text{C}}-\text{CH}=\text{CH}-\overset{\text{CH}_2}{\text{C}}=\text{CH}$), CHCHCHO ($\cdot\text{CH}=\text{CH}-\text{CH}=\text{O}$) and $\text{C}_4\text{H}_5\text{O}$ radicals. For CHCCHCHO and $\text{CH}_2\text{CHCHCHO}$, combinations with H atoms can give but-3-ynal (R42) and 3-butenal (R47), and with CH_3 radicals could lead to 2-methyl-but-3-ynal ($\text{CH}\equiv\text{C}-\underset{\text{CH}_3}{\text{CH}}-\text{CH}=\text{O}$, R43) and 2-methyl-3-butenal ($\text{CH}_2=\text{CH}-\underset{\text{CH}_3}{\text{CH}}-\text{CH}=\text{O}$, R48), while combinations of CHCHCHO and $\text{C}_4\text{H}_5\text{O}$ radicals with H radicals are sources of $\text{C}_2\text{H}_3\text{CHO}$ (R50) and dihydrofuran (, furan23H and , furan25H, R35-R37), respectively. The rate constants for these reactions were estimated as proposed by Allara et al. [36].

3.2 Secondary mechanism

The secondary mechanism includes the reactions of the primary products which are not considered in the mechanism of the oxidation of toluene [30], namely FA, methylfuran, but-3-ynal, 3-butenal, 2-methyl-but-3-ynal, 2-methyl-3-butenal, furan23H, furan25H and tetrahydrofuran (, THF). As discussed previously, FA can decompose to $\text{pC}_3\text{H}_4 + \text{CO}$ (R52), the rate constant of which has been determined using quantum calculations with CBS-QB3 method [32]. FA is also a source of C_3H_3 and CHO radicals (R51), the kinetics of which is from Sendt et al. [21] with the A-factor divided by 2.2 to take into account the pressure effect (for R1, the $k_\infty/k_{4.7\text{kPa}} = 2.2$ at 1000 K). In the case of methylfuran, the decomposition by breaking a C-H or C-O bond (R53-R60), bimolecular initiations with oxygen molecules (R61) and H-abstractions (R62-R71) are considered. The rate constants of these reactions were taken from Lifshitz et al. [40], except those of the bimolecular initiation with O_2 [46], and those reactions with O or C_2H_3 [47], with OH [48] and with HO_2 [49] which were obtained by analogy with toluene. For but-3-ynal, 3-butenal, 2-methylbut-3-ynal and 2-methyl3-butenal, the H-abstractions by H, OH and CH_3 radicals followed by decompositions (R79-R90) were taken into account, the kinetics of which were deduced from the similar reactions of

acetaldehyde [45,50,51].

For dihydrofuran and THF, the rates for their bimolecular reactions with oxygen (R91-R93, R118 and R119) were estimated from the correlation proposed by Ingham et al. [37] and those of metatheses reactions (R94-R108, R120-R129) were deduced from the correlations proposed by Heyberger et al. [39]. H-additions to dihydrofuran would give THF-2-yl (R109) and THF-3-yl (R110 and R111), respectively, and OH-additions would produce the same products HCHO + C₂H₄ + CHO (R112 and R113), the kinetics of which were from the correlations proposed by Heyberger et al. [39]. By β -scission, THF-2-yl and THF-3-yl could decompose to C₂H₄ + CH₂CHO (R114) and HCHO + C₃H₅ (R115), respectively, with the rates proposed by Sirjean et al. [52]. Terminations of the two tetrahydrofuryl radicals would form THF (R116 and R117), the kinetic data of which were estimated from the work of Allara and Shaw [36].

4. Results and Discussion

4.1 Experimental results

In this study, about 40 combustion intermediates, including hydrocarbons and oxygenated species, were detected and identified in the flames characterized by $\Phi = 1.4, 1.8$ and 2.2 . These species are listed in Table 4 along with the literature and measured IEs, peak concentrations and their locations in the flames. The detailed experimental data of mole fractions are available in supplemental material. To illustrate the effect of the equivalence ratio on the flame structure, Figures 4 to 8 present the temperature and concentration profiles. In Fig. 4, the temperature profiles are shown. Due to size of the thermocouple and its perturbation on the flame structure, the temperatures close to the burner (1.0 mm above) were extrapolated to the burner surface. As shown in Fig. 4, the flame temperatures steadily decrease and their peak locations shift downstream with the equivalence ratio increasing. In flame A, the maximum temperature is 1888 K located at 4.4 mm from the burner, while this value is decreased to 1772 K with a location of 6.2 mm in flame B and reaches 1699 K at 7.1 mm in flame C.

Mole fraction profiles of the major species including furan, O₂, Ar, H₂, H₂O, CO and CO₂ are

displayed as symbols in Fig. 5. The increase of the equivalence ratio in the furan flames causes a noticeable width increase of the reaction zone. In flame A, mole fraction of Ar remains constant after the position of 5.0 mm from the burner surface. This distance where Ar keeps constant shifts downstream to 7.0 mm in flame B and 9.0 mm at flame C. Among the three flames, both furan and O₂ consumed in further distances with the equivalence ratio increasing. The other major species, H₂, H₂O, CO and CO₂ have similar tendencies for the position with equilibrium value as that of Ar. In the post-flame zone, the mole fractions of Ar and CO₂ steadily decrease with the equivalence ratio increasing, while those of H₂ and CO show reverse trends. As evidenced from Fig. 5, the post flame H₂O levels were not sensitive to equivalence ratio. However, equivalence ratio has a significant impact on the X_{CO}/X_{CO₂} ratio. In the post-flame zone, the X_{CO}/X_{CO₂} ratio is about 1.2 for flame A. This ratio increases to 2.8 in flame B and reaches 8.3 in flame C.

Figures 6 to 8 display the mole fraction profiles of combustion intermediates in the furan flames. Generally, the peak positions of all these species are shifted downstream as Φ increases. Mole fraction profiles of C₁ – C₃ species are shown in Fig. 6. Methyl radical (CH₃) has peak-shaped mole fraction profiles in all investigated flames. Only a little variation is observed for the maximum concentration. As Φ increases from 1.4 to 2.2, the peak concentrations of methane (CH₄), acetylene (C₂H₂), propargyl radical (C₃H₃) and allene (aC₃H₄) are approximately doubled, while that of ethylene (C₂H₄) is multiplied by one and a half, and that of propyne (pC₃H₄) by a factor of 5. For allyl radical (C₃H₅), while, the difference in the maximum mole fraction observed in flame A and B is acceptable, the agreement strongly deteriorates in flame C.

The mole fraction profiles for C₄ – C₇ species presented in Fig. 7 also exhibit similar shift trends for the peak positions. With Φ increasing from 1.4 to 2.2, the maximum mole fractions of 1,2,3-butatriene/vinylacetylene (C₄H₄), 1,3-butadiene (C₄H₆), 1,3-cyclopentadiene (C₅H₆), 1,3,5-hexatriyne (C₆H₂) and benzene (C₆H₆) are approximately doubled, while that of diacetylene (C₄H₂) is multiplied by a factor of 5, and those of cyclopentadienyl radical (C₅H₅) and toluene (C₇H₈) are tripled. Thus, the equivalence ratio has the largest effect on the formation of C₄H₂. This can result

from the fact that C_2H_2 , the major precursor of C_4H_2 , is more abundantly formed as Φ increases.

Figure 8 shows the mole fraction profiles of the oxygenated intermediates. As Φ increases from 1.4 to 2.2, the peak concentration of 2-methylfuran is approximately doubled, while those of CH_2CO and methylketene/2-propenal (C_3H_4O) are multiplied by one and a half, and that of phenol (C_6H_5OH) by a factor of 10. Comparatively, the level of formaldehyde ($HCHO$) and ethanol/acetaldehyde (C_2H_4O) are not sensitive to equivalence ratio in the flame regime.

4.2 Kinetic modeling results

4.2.1 Simulation of the flame structure

The modeling of the chemical kinetics was performed using the CHEMKIN software [53], with the experimental temperature profiles introduced as input parameters for simulation. To account for the perturbations induced by the quartz probe and the thermocouple [54] and fit the experimental results, the temperature profile was shifted 1.5, 1.7 and 2.2 mm away from the burner surface for the flames with $\Phi = 1.4$, 1.8 and 2.2, respectively. The perturbation effect is known in molecular-beam mass spectroscopic investigations, and a shift equaling 4-5 times the orifice diameter has been reported for premixed low-pressure flames (4.0-5.0 kPa) [29,54,55].

The comparisons between the experimental measurements and predictions for the three flames are presented in Figs. 5-8, in which lines stand for simulated results. There is generally a reasonable agreement between measurements and predictions. For the major species shown in Fig. 5, the current model captures well the experimental values within the error limits. With Φ increasing from 1.4 to 2.2, the model also gives evidence of the increase of the reaction width, which is consistent with the measurements. The present mechanism overpredicts the formation of CO in flames A and B near the burner surface. The flux analysis indicates that CO is mainly formed by the reaction of O_2 with formyl radical (CHO) which is produced by addition of OH radical to the C=C double bond of furan. The too large formation of CO results from the too fast rate of the reaction $OH + furan$. The rate constant of this reaction needs to be more accurately determined by further experimental or theoretical studies. On the other hand, measurement uncertainties cannot be ruled out especially

since the reaction zone is narrower in flames A and B than that in flame C.

Figures 6 and 7 summarize the results for some selected $C_1 - C_7$ intermediates. Overall, the current model reproduces fairly well the mole fraction profiles of C_2H_2 , C_3H_3 , pC_3H_4 , C_3H_5 , C_4H_2 , C_4H_4 , C_4H_6 , C_5H_6 , C_6H_2 , C_6H_6 and C_7H_8 . The predicted peak concentration of CH_3 agrees well with the measurement in flame A. The present mechanism tends to overpredict the contributions from CH_3 in flames B and C. However, the agreement is still within the expected uncertainties (a factor of two for free radicals). In the post-flame zone, CH_3 has a too high predicted concentration, which is produced mainly from the reactions of H atom with pC_3H_4 , methanol (CH_3OH) and CH_2CO based on the rate-of-production (ROP) analysis. Compared to the reasonable capture of the CH_4 mole fraction shape for flames A and B, the current model exhibits a longer tail for flame C, which could be due to the reactions of abundant CH_3 with HCHO and CHO radical. With Φ increasing, the maximum mole fraction of C_2H_4 becomes larger and the peak position shifts further. While the simulated mole fraction profiles of C_2H_4 have the same tendencies as the experimental measurements, the peak values are underpredicted in flames A and B. The ROP analysis at the peak positions indicates that C_2H_4 is mainly formed by the reactions of CH_2CO+CH_2 and C_2H_3CHO+H in all three flames. Note that the formation of ethane (C_2H_6) is negligible in all three flames. As revealed by the ROP analysis, C_2H_6 is mainly formed through the combination of CH_3 radicals and most of C_2H_6 converts to C_2H_5 radical and finally to C_2H_4 . For aC_3H_4 , the current model gives fairly reasonable predictions in flames A and B, but a poor one in flame C. According to the ROP analysis result, most of aC_3H_4 comes from C_3H_5 . As seen Fig. 6 (h), the maximum mole fraction of C_3H_5 is somewhat overpredicted in flames B and C, which could then lead to the overprediction of aC_3H_4 .

It should be noted that in flame C, the maximum mole fraction of C_4H_2 is about 2.5 times overpredicted. By checking the ROP result, the reaction $C_2H_2 + C_2H$ accounts for more than 80% of C_4H_2 formation. As C_2H_2 is satisfactorily predicted, this disagreement could result from an experimental error. For mass 52 represented in Fig. 7(b), the PIE spectra indicate that it involves the contribution of both 1,2,3-butatriene and vinylacetylene. According to the modeling result, the ratios

of their maximum mole fraction $X_{\text{vinylacetylene}}/X_{1,2,3\text{-butatriene}}$ are 8.8, 8.2 and 4.9 in flames A, B and C, respectively, which demonstrates that vinylacetylene is the dominant species. The ROP result shows that about 70% vinylacetylene comes from the reaction of C_3H_3 with triplet CH_2 . As seen in Fig. 7(d), the ratio of the experimental and predicted peak mole fraction for C_5H_5 is within 0.5 ~ 2.0. Considering the experimental and modeling uncertainties, mole fraction profiles of both species are determined accurately enough by the current model. In flame A, the metatheses of 1,3-cyclopentadiene with H and decomposition of phenoxy radical accounts for 45% and 33% C_5H_5 formation, respectively. However, decomposition of phenoxy radical is the major source (81%) of C_5H_5 in flame C. The predicted peak values of the two C_6H_6 isomers, benzene and fulvene (vC_6H_6) reveals that benzene is dominant for mass 78, which is in agreement with experimental observations. An increase after the peak value is observed for the predicted C_7H_8 profile in flame C. This phenomenon is caused by the combination of C_6H_5 radical with CH_3 radical which is abundantly predicted in the post flame zone of flame C.

In Fig. 8, the comparison between the measured and modeled oxygenated combustion intermediates are presented. Contributions from CH_2CO , C_5H_6O and C_6H_5OH are correctly reproduced. Both the measurement and simulation show that HCHO is an abundant oxygenated intermediate in all the three flames. While the predicted shape and maximum mole fraction of HCHO are close to the measurements in flame A, the maximum mole fractions are somewhat overpredicted in flames B and C. For C_2H_4O , the peak positions are predicted correctly. As Φ increases from 1.4 to 2.2, the predicted maximum mole fraction of C_2H_4O decreases. The current model only captures C_2H_4O reasonably in flame C. As revealed from the ROP analysis, an important part of the formation of C_2H_4O in flames A and B comes from the combination of CH_3 and CHO radicals. When CHO radicals are excessively formed through the reaction of $OH + \text{furan}$, a excess of C_2H_4O can be produced. The current model tends to overpredict the C_3H_4O contribution in the three flames, which could result from an inaccurate estimation of the photoionization cross section of C_3H_4O . The ROP result indicates that C_3H_4O is mainly formed by the addition of OH to furan in

both flame A (81%) and C (82%).

It is obvious that there are some discrepancies between the predictions of the present model and the experimental measurements, especially for intermediates such as CH_3 , CH_4 , C_2H_4 , C_4H_2 and benzene in flame C. The uncertain rate constants of some reactions, for instance, $\text{furan} + \text{OH} = \text{C}_2\text{H}_3\text{CHO} + \text{CHO}$ (correlated with similar reaction) and $\text{CH}_2\text{CCHCHO} = \text{C}_3\text{H}_3 + \text{CHO}$ (considered the pressure effect) could cast influence on the predictions. Moreover, the estimation of photoionization cross section for some intermediates can be another issue of the disagreement. As the current model is the first attempt to simulate the furan oxidation under flame conditions, further flame data are desirable for the validation of the present mechanism.

4.2.2 Rate-of-production and sensitivity analysis for furan consumption in flames

To illustrate the major reaction channels of furan, flux analysis has been performed for two equivalence ratios 1.4 (flame A, at 3.7 mm from the burner, $T = 1470$ K, 88.9% furan conversion) and 2.2 (flame C, at 7.9 mm from the burner, $T = 1609$ K, 85.0% furan conversion). As presented in Fig. 9, the major routes are quite different between the two flames. Metatheses by H, O and OH to produce furyl-2 and furyl-3 radicals account for about 26.8% of furan consumption in flame C, while this value is as high as 47.2% in flame A. Both furyl-2 and furyl-3 radicals are consumed mainly by decomposition via β -scission, giving $\text{CH}=\text{CH}-\text{CH}=\text{C}=\text{O}$ and $\text{CH}\equiv\text{C}-\text{CH}=\text{CH}-\text{O}$ radicals, respectively. By β -scission, $\text{CH}=\text{CH}-\text{CH}=\text{C}=\text{O}$ radicals are completely converted to C_2H_2 and HCCO radicals, which is an important source of C_2H_2 . In both flames A and C, most of the $\text{CH}\equiv\text{C}-\text{CH}=\text{CH}-\text{O}$ radicals decompose to give $\text{C}_3\text{H}_3 + \text{CO}$ (1,2-H transfer followed by a fast C-O bond dissociation) and $\text{CH}\equiv\text{C}-\text{CH}=\text{C}=\text{O} + \text{H}$, as displayed in Fig. 2.

While the reaction $\text{furan} = \text{FA}$ accounts for 35.7% of furan conversion in flame C, it plays a less significant role (only 3.5%) in flame A. This results from the characteristics of flame C being closer to pyrolysis conditions under which thermal decomposition reactions have more important influence on the furan consumption than that in flame A. FA is consumed dominantly by decomposition to C_3H_3 and HCO radicals and only about one-third goes to $\text{CO} + \text{pC}_3\text{H}_4$ in flame C, while it is the

reverse case in flame A. It should be noted that the addition of OH to the C=C bond forming $C_3H_4O + HCO$ is also important for furan consumption. More than 15% furan in flame A and about 6% furan in flame C decompose via this pathway.

In general, H-additions of furan forming C_4H_5O radicals account for about 20% of furan consumption in both flame A and C. The C_4H_5O-2 and C_4H_5O-3 radicals are finally converted to $C_2H_2 + CH_2CHO$ and $CO + C_3H_5$. In addition, unimolecular decomposition of furan to $C_2H_2 + CH_2CO$ accounts for 7.1% of furan consumption in flame C. However, this reaction has a less important effect on furan consumption (1%) than the other pathways in flame A.

To identify the reactions that serve as bottle-necks in the consumption of furan, a local sensitivity analysis has been performed with the proposed mechanism for the flames A and C, as displayed in Fig. 10. For brevity, C_0-C_2 reactions are not shown except for $O_2 + H = OH + O$ which has the most important promoting effect. The sensitivity analysis indicates that the reaction furan = FA (R1) plays the key role for furan consumption in flame C. The addition of OH radical to furan giving C_2H_3CHO and CHO radical has a similar promoting effect in both flames. The decomposition of C_4H_5O-2 to give C_2H_2 and CH_2CHO radical, and the metatheses of furan with H/OH radicals to yield furyl-2/furyl-3 have a more important promoting effect in flame A than in flame C. The decompositions of FA to give CHO and C_3H_3 , $CHCCHCHO$ to H atom and $CHCCHCO$, the unimolecular decomposition of furan to yield C_2H_2 and CH_2CO , the metatheses of furan with O-atoms, and the ipso-addition of methyl radicals to produce methylfuran, also have a promoting effect in flame C. However, these reactions have no visible effect in flame A. The decomposition of FA to give CO and pC_3H_4 has a strong inhibiting effect on furan consumption in flame C. In the case of flame A, the decomposition of $CH_2CHCHCHO$ to give CO and C_3H_5 radical plays a key role in the inhibition of furan consumption. While the addition of H atom to furan giving C_4H_5O-3 , the H-additions to C_4H_5O-3 forming dihydrofuran, and the combination of H atom with $CHCCHCHO$ to give $CHCCH_2CHO$, have only a slight inhibiting effect in flame A and no effect in flame C, the reaction $CHCCHCHO = CO + C_3H_3$ has a reverse tendency.

4.2.3 Aromatic formation

Among the products of furan pyrolysis analyzed by Winkler et al. [16], a lot of aromatic species such as naphthalene, phenanthrene, pyrene and acenaphthylene were identified. However, even under the richest condition (flame C), only benzene, toluene, phenylacetylene (C_8H_6) and styrene (C_8H_8) were identified in the present work. This could be due to the relatively low temperature of the studied flames, as well as to the existence of O atom in furan, hindering the formation of much larger aromatics. In the following section, we will focus on the formation pathways of these species, based on the flux analysis taken at the same positions as mentioned in 4.2.2.

For all the investigated flames, the reaction fulvene + H = C_6H_6 + H is an important formation channel of C_6H_6 (36.1% for flame A and 24.2% for flame C), where fulvene is mostly formed by the combination of C_3H_3 radicals and by reaction between C_3H_3 and C_3H_5 radicals. Besides this reaction, the combination of C_3H_3 radicals is another significant source of C_6H_6 (23.4% for flame A and 71.9% for flame C). The ipso-addition of H atom to C_6H_5OH (27.8%) and the reaction $C_6H_5 + H (+M) = C_6H_6 (+M)$ (6.2%) also contribute to the C_6H_6 formation in flame A. However, these two reactions have no contribution to C_6H_6 production in flame C. The flux analysis indicates that the formation pathway of toluene is not sensitive to the equivalence ratio. It is dominated by the combination reaction $C_6H_5 + CH_3$ (56.5% for flame A and 91.8% for flame C), in which C_6H_5 radicals are dominantly generated from the combination of C_3H_3 radicals. In contrast, the reaction toluene = benzyl + H is also important for toluene production in flame A (39.6%), but it is a consumption route in flame C. In flame C, C_8H_6 is formed mainly by the reactions of C_2H_2 and C_4H_2 with C_6H_5 radicals, and C_8H_8 is produced mainly by the decomposition of 2-phenylethyl radicals and by the combination reaction $C_6H_5 + C_2H_3$.

4.2.4 Validation of the present mechanism using pyrolysis results

To extend the validity of the present mechanism, previous pyrolysis results from Organ and Mackie (20.0 atm with initial furan concentration of 2.0%, 1.0% and 0.2% dilute in Ar) [14] and Fulle et al. (0.26 atm with furan concentration of 2.0% dilute in Ne) [15] were modeled. Considering

that the pressures used in pyrolysis experiments are higher than in the flames, high pressure rate constants for reactions R1, R2, R51 and R52 that were calculated using quantum calculations with CBS-QB3 method [32] have been used in simulations.

Figure 11 compares the predicted furan and product profiles with the experimental results (shock tube, residence time 300 μ s) reported by Organ and Mackie [14], in which symbols are measurements and solid, dash dot and dashed lines are respective predictions by the current model for 2.0%, 1.0% and 0.2% initial furan concentration. Also, the predictions for 2.0% initial furan concentration by the mechanism of Sendt et al. [21] are given for comparison. In general, the present model gives acceptable agreement with experimental furan profile. Particularly, in the temperature range 1450 – 1550 K, the current predictions are slightly closer to the measurements than those obtained with the model of Sendt et al. [21]. Good agreement is also obtained for C_2H_2 , C_3H_4 and C_6H_6 . When the temperature is higher than 1500 K, CO is somewhat underpredicted by the present mechanism under all inlet conditions. This underprediction is also observed by the model of Sendt et al. [21]. While the model of Sendt et al. [21] gave underprediction of the minor product CH_4 in the temperature range > 1500 K, the current model also tends to underpredict CH_4 under all inlet conditions. As indicated from the ROP analysis, CH_4 is mainly formed by the reaction of CH_3 radicals with C_3H_4 . Since C_3H_4 is reasonably well predicted, the underprediction of CH_4 can be due to the consumption of CH_3 radicals through the reaction furan + CH_3 = methylfuran + H. C_2H_4 is fairly predicted for 0.2% inlet condition with the present mechanism. However, it is underpredicted for 2% and 1% inlet conditions, which also can result from a too large consumption of CH_3 radicals, which are a key source of C_2H_4 ($CH_3 \leftrightarrow C_2H_4 \leftrightarrow C_2H_6$). The model of Sendt et al. [21] shows worse prediction of C_3H_4 than ours in the temperature range of 1450 – 1525 K, but better prediction when the temperature is higher than 1525 K.

Figure 12 shows the flux analysis result for 2.0% initial furan concentration at 1527 K, corresponding to 64.8% of furan conversion, at which both propyne and benzene have peak mole fractions experimentally. As noted in the result of Sendt et al. [21], their model supported a

mechanism involving two parallel furan decomposition routes to the major products $\text{CO} + \text{pC}_3\text{H}_4$ and $\text{C}_2\text{H}_2 + \text{CH}_2\text{CO}$, which is exactly the same as observed in this work. As seen in Fig. 12, furan is mainly converted to FA, which is also the same as that observed in flame C. Under pyrolysis conditions, the main products from FA are $\text{pC}_3\text{H}_4 + \text{CO}$, while most FA gives $\text{C}_3\text{H}_3 + \text{HCO}$ in flame C. Besides to FA, decomposition to $\text{C}_2\text{H}_2 + \text{CH}_2\text{CO}$ is another important consumption pathway of furan pyrolysis (25.2%). However, this channel is a minor pathway in flames even under the richest condition. In addition, 7.8% of furan disappears by reactions with H and CH_3 radicals, forming methylfuran, furyl-2, furyl-3, $\text{C}_4\text{H}_5\text{O-2}$ and $\text{C}_4\text{H}_5\text{O-3}$ radicals. Furyl-2 can decompose to $\text{C}_2\text{H}_2 + \text{HCCO}$ and $\text{CH}=\text{C}-\text{CH}=\text{C}=\text{O} + \text{H}$ via $\text{CH}=\text{CH}-\text{CH}=\text{C}=\text{O}$ radical. By β -scission to $\text{CH}\equiv\text{C}-\text{CH}=\text{CH}-\text{O}$, furyl-3 can give $\text{C}_3\text{H}_3 + \text{CO}$ and $\text{CH}\equiv\text{C}-\text{CH}=\text{C}=\text{O} + \text{H}$. In contrast, the pathway to $\text{CH}\equiv\text{C}-\text{CH}=\text{C}=\text{O} + \text{H}$ from $\text{CH}=\text{CH}-\text{CH}=\text{C}=\text{O}$ is not observed from the flame studies. Moreover, $\text{C}_4\text{H}_5\text{O-2}$ and $\text{C}_4\text{H}_5\text{O-3}$ finally produce $\text{C}_2\text{H}_2 + \text{CH}_2\text{CHO}$ and $\text{C}_3\text{H}_5 + \text{CO}$, respectively, while the formations of these two radicals are much more involved in the consumption of furan in the flames.

Figure 13 presents the comparison of the predicted furan and product profiles with the experimental results (2% furan/98% Ne, 1533 K, 198 Torr) reported by Fulle et al. [15], in which symbols are measured data and solid and dash lines are respective predictions by the current model and the mechanism of Fulle et al. [15]. Although CO and propyne are underpredicted slightly at the end of the observation period, a globally correct prediction can be observed for the current model. It should be noted that no other products were detected within the period of $\sim 800 \mu\text{s}$ and only the two unimolecular dissociation reactions were involved in the model of Fulle et al. [15]. They also determined the ratio $[\text{C}_2\text{H}_2]/[\text{CO}]$ and gave an expression $[\text{C}_2\text{H}_2]/[\text{CO}] = (5.5 \cdot 10^{-9}) T^{2.5}$ by fitting their own results and that of Lishitz et al. [12]. In this work, the predicted ratios of $[\text{C}_2\text{H}_2]/[\text{CO}]$ are 0.45 at $400 \mu\text{s}$ and 0.44 at $800 \mu\text{s}$, which are very close to respective 0.42 and 0.40 that are calculated using the fitted expression of Fulle et al. [15].

To analyze the difference of the rate constants calculated in this work for furan pyrolysis, it is necessary to compare them with previous measurements and calculations, as displayed in Fig. 14.

The unimolecular reactions for furan pyrolysis are commonly accepted as dissociation to $\text{CO} + \text{pC}_3\text{H}_4$ and $\text{C}_2\text{H}_2 + \text{CH}_2\text{CO}$ [12,14,15,18,21], while $\text{CO} + \text{pC}_3\text{H}_4$ is dominant at temperatures lower than 1270 K [11,13]. At temperatures higher than 1550 K, furan can generate C_3H_3 [18]. As seen in Fig. 14, only the total reaction, including routes of $\text{CO} + \text{pC}_3\text{H}_4$ and $\text{C}_2\text{H}_2 + \text{CH}_2\text{CO}$ are considered. In the current model and mechanism of Sendt et al. [21], the reaction furan = FA is used since it is the rate-determining step to form $\text{CO} + \text{pC}_3\text{H}_4$. Generally, the rate constant of this work is in good agreement with previous ones predicted by Lishitz et al. [12], Bruinsma et al. [13], Organ and Mackie [14] and Sendt et al. [21]. The low-temperature rate constants given by Grela et al. [11] are higher than the current model and measurements of Organ and Mackie [14], which was also observed by Sendt et al. [21]. The model of Fulle et al. [15] showed good agreement with the present mechanism at temperatures higher than 1300 K, but displays a slightly lower rate constant than the current ones at lower temperatures.

5. Conclusions

An experimental and numerical investigation has been conducted to analyze the chemical structures of three low-pressure premixed furan/ O_2 /Ar flames with tunable synchrotron VUV photoionization and molecular-beam mass spectrometry. About 40 combustion intermediates and products have been identified by measurements of photoionization efficiency spectra. Mole fractions of the flame species have been calculated. A detailed furan combustion model has been developed and reasonable agreement has been obtained between experimental measurements and simulations. The current mechanism has also been successfully validated against previous data obtained for furan pyrolysis. However, further studies still remain to improve this first attempt of mechanism for the combustion of furan.

In flames, the width of the reaction zone is increased and the peak positions of most intermediates are shifted downstream with the equivalence ratio increasing; furan is consumed mainly by metatheses leading to furyl radicals, OH addition to the double bond of furan giving 2-

propenal and $\text{CH}=\text{CH}-\text{CHO}$ radicals by β -scission, isomerization forming formyl allene via 1,2-hydrogen migration; benzene is formed mainly by isomerization of fulvene which comes from the combination of the propargyl radicals. A sensitivity analysis indicates that the reaction $\text{furan} = \text{CH}_2\text{CCHCHO}$ has a strong promoting effect, while the decomposition of CH_2CCHCHO to CO and pC_3H_4 in flame with $\Phi = 1.4$, and $\text{CH}_2\text{CHCHCHO}$ to CO and C_3H_5 radical in flame with $\Phi = 2.2$ have strong inhibiting effects on furan decomposition. Under pyrolysis conditions, the major decomposition products of furan are $\text{CO} + \text{pC}_3\text{H}_4$ and $\text{C}_2\text{H}_2 + \text{CH}_2\text{CO}$. Moreover, the present rate constants of furan dissociation at high pressures based on ab initio calculations are in good agreement with previous experimental measurements and calculations.

ACKNOWLEDGMENTS

This work performed by CNRS-Nancy University was funded by the European Commission through the “Clean ICE” Advanced Research Grant of the European Research Council. FQ is grateful for the funding supports from Chinese Academy of Sciences, Natural Science Foundation of China (50925623), and Ministry of Science and Technology of China (2007DFA61310). This work was granted access to the HPC resources of CINES under the allocation 2010- [c2010086030] made by GENCI (Grand Equipement National de Calcul Intensif).

References

- [1] K. Kohse-Höinghaus, P. Oßwald, T.A. Cool, T. Kasper, N. Hansen, F. Qi, C.K. Westbrook, P.R. Westmoreland, *Angew. Chem. Int. Edit.* 49 (2010) 3572-3598.
- [2] Y. Román-Leshkov, C.J. Barrett, Z.Y. Liu, J.A. Dumesic, *Nature* 447 (2007) 982-985.
- [3] Avantium: Avantium steps ahead with its biofuels program-engine test demonstrates potential of "furanics", <http://www.avantium.com>, October 22, 2007.
- [4] M.O. Andreae, P. Merlet, *Global Biogeochem. Cy.* 15 (2001) 955-966.
- [5] P. Ciccioli, E. Brancaleoni, M. Frattoni, A. Cecinato, L. Pinciarelli, *Anal. Lett.* 34 (2001) 937-955.
- [6] T.G. Karl, T.J. Christian, R.J. Yokelson, P. Artaxo, W.M. Hao, A. Guenther, *Atmos. Chem. Phys. Discuss.* 7 (2007) 8755-8793.
- [7] J.P. Greenberg, H. Friedli, A.B. Guenther, D. Hanson, P. Harley, T. Karl, *Atmos. Chem. Phys.* 6 (2006) 81-91.
- [8] G. Holzner, J. Oró, W. Bertsch, *J. Chromatogr.* 126 (1976) 771-785.
- [9] F. Guarneri, E. Ikeda, J.C. Mackie, *Energy & Fuels* 15 (2001) 743-750.
- [10] C.F. Cullis, A.C. Norris, *Carbon* 10 (1972) 525-537.
- [11] M.A. Grela, V.T. Amorebieta, A.J. Colussi, *J. Phys. Chem.* 89 (1985) 38-41.
- [12] A. Lifshitz, M. Bidani, S. Bidani, *J. Phys. Chem.* 90 (1986) 5373-5377.
- [13] O.S.L. Bruinsma, P.J.J. Tromp, H.J.J.d.S. Nolting, J.A. Moulijn, *Fuel* 67 (1988) 334-340.
- [14] P.P. Organ, J.C. Mackie, *J. Chem. Soc. Faraday Trans.* 87 (1991) 815-823.
- [15] D. Fulle, A. Dib, J.H. Kiefer, Q. Zhang, J. Yao, R.D. Kern, *J. Phys. Chem. A* 102 (1998) 7480-7486.
- [16] J.K. Winkler, W. Karow, P. Rademacher, *J. Anal. Appl. Pyrol.* 57 (2001) 133-144.
- [17] N.R. Hore, D.K. Russell, *New J. Chem.* 28 (2004) 606-613.
- [18] A. Vasiliou, M.R. Nimlos, J.W. Daily, G.B. Ellison, *J. Phys. Chem. A* 113 (2009) 8540-8547.
- [19] R.F. Liu, X.F. Zhou, L. Zhai, *J. Comput. Chem.* 19 (1998) 240-249.
- [20] R.F. Liu, X.F. Zhou, T.M. Zuo, *Chem. Phys. Lett.* 325 (2000) 457-464.
- [21] K. Sendt, G.B. Bacskay, J.C. Mackie, *J. Phys. Chem. A* 104 (2000) 1861-1875.
- [22] C.Q. Huang, B. Yang, R. Yang, J. Wang, L.X. Wei, X.B. Shan, L.S. Sheng, Y.W. Zhang, F. Qi, *Rev. Sci. Instrum.* 76 (2005) 126108.
- [23] C.A. Taatjes, N. Hansen, A. McIlroy, J.A. Miller, J.P. Senosiain, S.J. Klippenstein, F. Qi, L.S. Sheng, Y.W. Zhang, T.A. Cool, J. Wang, P.R. Westmoreland, M.E. Law, T. Kasper, K. Kohse-Hoinghaus, *Science* 308 (2005) 1887.

- [24] Y.Y. Li, F. Qi, *Acc. Chem. Res.* 43 (2010) 68-78.
- [25] F. Qi, R. Yang, B. Yang, C.Q. Huang, L.X. Wei, J. Wang, L.S. Sheng, Y.W. Zhang, *Rev. Sci. Instrum.* 77 (2006) 084101.
- [26] T.A. Cool, K. Nakajima, C.A. Taatjes, A. McIlroy, P.R. Westmoreland, M.E. Law, A. Morel, *Proc. Combust. Inst.* 30 (2005) 1681.
- [27] M. Kamphus, N.N. Liu, B. Atakan, F. Qi, A. McIlroy, *Proc. Combust. Inst.* 29 (2002) 2627-2633.
- [28] R.M. Fristrom, *Flame Structure and Processes*, Oxford, New York, 1995.
- [29] Z.Y. Tian, Y.Y. Li, L.D. Zhang, P. Glarborg, F. Qi, *Combust. Flame* 156 (2009) 1413-1426.
- [30] Z.Y. Tian, W.J. Pitz, R. Fournet, P.A. Glaude, F. Battin-Leclerc, *Proc. Combust. Inst.* 33 (2010) doi:10.1016/j.proci.2010.06.063.
- [31] C. Muller, V. Michel, G. Scacchi, G.M.Côme, *J. Chim. Phys.* 92 (1995) 1154-1177.
- [32] J.A. Montgomery, M.J. Frisch, J.W. Ochterski, G.A. Petersson, *J. Chem. Phys.* 110 (1999) 2822-2827.
- [33] M. J. Frisch and et al. *Gaussian03*, revision B05; Gaussian, Inc.: Wallingford, CT, 2004.
- [34] V. Mokrushin, W. Tsang, *Chemrate v.1.5.2*; NIST, Ed. Gaithersburg, MD 20899, U.S.A., 2006.
- [35] A.V. Joshi, H. Wang, *Int. J. Chem. Kinet.* 38 (2006) 57-73.
- [36] D.L. Allara, R.J. Shaw, *J. Phys. Chem. Ref. Data* 9 (1980) 523-559.
- [37] T. Ingham, R.W. Walker, R.E. Woolford, *Proc. Combust. Inst.* 25 (1994) 767-774.
- [38] H.A. Gueniche, P.A. Glaude, R. Fournet, F. Battin-Leclerc, *Combust. Flame* 151 (2007) 245-261.
- [39] B. Heyberger, N. Belmekki, V. Conraud, P.A. Glaude, R. Fournet, F. Battin-Leclerc, *Int. J. Chem. Kinet.* 34 (2002) 666-677.
- [40] A. Lifshitz, C. Tamburu, R. Shashua, *J. Phys. Chem. A* 101 (1997) 1018-1029.
- [41] K.M. Leung, R.P. Lindstedt, *Combust. Flame* 102 (1995) 129-160.
- [42] A.M. Mebel, E.W.G. Diau, M.C. Lin, K. Morokuma, *J. Am. Chem. Soc.* 118 (1996) 9759-9771.
- [43] P. Dagaut, J.C. Boettner, M. Cathonnet, *Combust. Sci. Technol.* 77 (1991) 127-148.
- [44] S. Touchard, R. Fournet, P.A. Glaude, V. Warth, F. Battin-Leclerc, G. Vanhove, M. Ribaucour, R. Minetti, *Proc. Combust. Inst.* 30 (2005) 1073-1081.
- [45] D.L. Baulch, C.J. Cobos, R.A. Cox, P. Frank, G. Hayman, Th. Just, J.A. Kerr, T. Murrells, M.J. Pilling, J. Troe, R.W. Walker, J. Warnatz, *Combust. Flame* 98 (1994) 59-79.
- [46] M.A. Oehlschlaeger, D.F. Davidson, R.K. Hanson, *Combust. Flame* 147 (2006) 195-208.

- [47] W.J. Pitz, R. Seiser, J.W. Bozzelli, I. Da Costa, R. Fournet, F. Billaud, F. Battin-Leclerc, K. Seshadri, C.K. Westbrook, in Proceedings of the 2nd Joint Meeting of the U.S. Sections of the Combustion Institute, 2001.
- [48] R. Knispel, R. Koch, M. Siese, C. Zetsch, Ber. Bunsen-Ges. Phys. Chem. 94 (1990) 1375-1379.
- [49] M. Mehl, A. Frassoldati, R. Fietzek, W.J.P. T. Faravelli, E. Ranzi, in Fall Technical Meeting of the Western States Section of the Combustion Institute, Irvine, CA, 2009.
- [50] J. Warnatz, Rate coefficients in the C/H/O system, Combustion Chemistry, W.C. Gardiner, Jr. (Ed.), Springer-Verlag, 1984.
- [51] J. Cavanagh, R.A. Cox, G. Olson, Combust. Flame 82 (1990) 15-39.
- [52] B. Sirjean, F. Buda, H. Hakka, P.A. Glaude, R. Fournet, F. Battin-Leclerc, Proc. Combust. Inst. 31 (2007) 277-284.
- [53] R.J. Kee, J.F. Grcar, M.D. Smooke, J.A. Miller, Sandia Report: SAND85-8240, 1985.
- [54] U. Struckmeier, P. Oßwald, T. Kasper, L. Böling, M. Heusing, M. Köhler, A. Brockhinke, K. Kohse-Höinghaus, Z. Phys. Chem. Neue Folge 223 (2009) 503-537.
- [55] A. Bhargava, P.R. Westmoreland, Combust. Flame 113 (1998) 333-347.
- [56] V. Warth, N. Stef, P.A. Glaude, F. Battin-Leclerc, G. Scacchi, G.M. Côme, Combust. Flame 114 (1998) 81-102.
- [57] K. Brezinsky, T.A. Litzinger, I. Glassman, Int. J. Chem. Kinet. 16 (1984) 1053-1074.
- [58] R. Bounaceur, I. Da Costa, R. Fournet, F. Billaud, F. Battin-Leclerc, Int. J. Chem. Kinet. 37 (2005) 25-49.
- [59] P.J. Linstrom, W.G. Mallard, <http://webbook.nist.gov/chemistry> (2003) NIST Standard Reference Database Number 69.
- [60] X.S. Wu, Z.H. Huang, T. Yuan, K.W. Zhang, L.X. Wei, Combust. Flame 156 (2009) 1365-1376.

Table 1 Flame characteristics

Flame	Φ^a	Flowrate (SLM)			C/O	D_M^b (g/s/cm ²)
		Furan	O ₂	Ar		
A	1.4	0.328	1.053	1.000	0.538	2.526E-3
B	1.8	0.395	0.986	1.000	0.667	2.590E-3
C	2.2	0.453	0.928	1.000	0.786	2.646E-3

Notes: ^a Φ refers to the equivalence ratio; ^b D_M is the mass flow rate of the gas mixture.

Table 2 Reactions of furan and derived species

Reaction	A	n	E _a	Footnote	No.	
PRIMARY MECHANISM						
Reactions of furan						
Unimolecular initiations by breaking of a C-O or C-H bond						
Furan = FA	(P = 4.7 kPa)	6.0×10^{58}	-13.388	94.0	a	(1)
	(P → ∞)	2.3×10^{12}	0.416	70.891	a	(1')
Furan = C ₂ H ₂ + CH ₂ CO	(P = 4.7 kPa)	3.8×10^{73}	-17.412	113.3	a	(2)
	(P → ∞)	1.8×10^{14}	0.534	86.591	a	(2')
Furyl-2 + H = furan		1.0×10^{14}	0.0	0.0	b	(3)
Furyl-3 + H = furan		1.0×10^{14}	0.0	0.0	b	(4)
Bimolecular initiations						
Furan + O ₂ = furyl-2 + HO ₂		2.0×10^{13}	0.0	70.68	c	(5)
Furan + O ₂ = furyl-3 + HO ₂		2.0×10^{13}	0.0	70.88	c	(6)
Additions and decompositions						
Furan + H = C ₄ H ₅ O-2		2.6×10^{13}	0.0	3.2	d	(7)
Furan + H = C ₄ H ₅ O-3		2.6×10^{13}	0.0	1.56	d	(8)
Furan + OH = C ₂ H ₃ CHO + CHO		2.7×10^{12}	0.0	-1.04	e	(9)
Methylfuran + H = furan + CH ₃		5.0×10^{14}	0.0	8.0	f	(10)
Metatheses						
Furan + H = furyl-2 + H ₂		8.2×10^5	2.5	12.28	e	(11)
Furan + H = furyl-3 + H ₂		8.2×10^5	2.5	12.28	e	(12)
Furan + O = furyl-2 + OH		1.2×10^{11}	0.7	8.96	e	(13)
Furan + O = furyl-3 + OH		1.2×10^{11}	0.7	8.96	e	(14)
Furan + OH = furyl-2 + H ₂ O		2.2×10^6	2.0	2.78	e	(15)
Furan + OH = furyl-3 + H ₂ O		2.2×10^6	2.0	2.78	e	(16)
Furan + CH ₃ = furyl-2 + CH ₄		1.4×10^0	3.5	12.9	e	(17)
Furan + CH ₃ = furyl-3 + CH ₄		1.4×10^0	3.5	12.9	e	(18)
Reactions of furyl radicals (cyclo-C ₄ H ₃ O)						
Isomerization						
Furyl-3 = furyl-2		1.5×10^{13}	0.0	67.8	g	(19)
Decompositions by β-scission						
Furyl-2 = CHCHCHCO		1.8×10^{13}	0.341	34.511	a	(20)
Furyl-3 = CHCCHCHO		1.1×10^{13}	0.306	31.215	a	(21)
Oxidations						
Furyl-2 + O ₂ = CH ₂ CHCO + CO ₂		4.5×10^{16}	-1.39	1.0	h	(22)
Furyl-2 + O ₂ => CHCHCHO + CO + O		3.3×10^{11}	-0.29	10.0	h	(23)
Furyl-3 + O ₂ = CH ₂ CHCO + CO ₂		4.5×10^{16}	-1.39	1.0	h	(24)
Furyl-3 + O ₂ => C ₂ H ₂ + CHO + CO + O		3.3×10^{11}	-0.29	10.0	h	(25)
Combinations						
Furyl-2 + O = CHCHCHO + CO		3.0×10^{13}	0.0	0.0	i	(26)
Furyl-3 + O = CHCHCHO + CO		3.0×10^{13}	0.0	0.0	i	(27)
Reactions of cyclo-C ₄ H ₅ O						
Isomerization						
C ₄ H ₅ O-2 = C ₄ H ₅ O-3		3.3×10^9	1.0	39.1	j	(28)
Decompositions by β-scission						
C ₄ H ₅ O-2 = C ₂ H ₂ +CH ₂ CHO		8.1×10^{12}	0.246	34.925	a	(29)
C ₄ H ₅ O-3 = CH ₂ CHCHCHO		1.1×10^{13}	0.085	22.555	a	(30)
Reactions with O ₂						
C ₄ H ₅ O-2 + O ₂ = furan + HO ₂		2.6×10^{11}	0.0	2.5	k	(31)
C ₄ H ₅ O-3 + O ₂ = furan + HO ₂		1.6×10^{12}	0.0	15.2	k	(32)
Combinations						
C ₄ H ₅ O-2 + O = C ₂ H ₃ CHO + CHO		5.5×10^{13}	0.0	0.0	l	(33)
C ₄ H ₅ O-3 + O = C ₂ H ₂ + HCHO + CHO		5.5×10^{13}	0.0	0.0	l	(34)
C ₄ H ₅ O-2 + H = furan23H		1.0×10^{14}	0.0	0.0	b	(35)
C ₄ H ₅ O-3 + H = furan23H		1.0×10^{14}	0.0	0.0	b	(36)
C ₄ H ₅ O-3 + H = furan25H		1.0×10^{14}	0.0	0.0	b	(37)
Reactions of C ₄ H ₃ O						
Decompositions by β-scission						
CHCHCHCO = C ₂ H ₂ + CHCO		5.3×10^{15}	-0.234	34.234	a	(38)
CHCHCHCO = CHCCHCO + H		8.7×10^{11}	0.706	38.680	a	(39)

CHCCHCHO = CO + C ₃ H ₃		1.5×10^{12}	0.345	48.401	a	(40)
CHCCHCHO = CHCCHCO + H		1.0×10^{12}	0.725	51.949	a	(41)
Combinations						
CHCCHCHO + H = CHCCH ₂ CHO		1.0×10^{14}	0.0	0.0	b	(42)
CHCCHCHO + CH ₃ = C ₃ H ₆ O		1.5×10^{13}	0.0	0.0	m	(43)
Reactions of C ₄ H ₅ O						
Isomerization						
CH ₂ CHCHCHO = CHCHCHCHOH		2.2×10^{11}	0.435	35.127	a	(44)
Decompositions by β-scission						
CH ₂ CHCHCHO = CO + C ₃ H ₅		4.9×10^{12}	0.261	47.443	a	(45)
CHCHCHCHOH = C ₂ H ₂ + CH ₂ CHO		1.2×10^{15}	0.102	48.750	a	(46)
Combinations						
CH ₂ CHCHCHO + H = CH ₂ CHCH ₂ CHO		1.0×10^{14}	0.0	0.0	b	(47)
CH ₂ CHCHCHO + CH ₃ = C ₃ H ₈ O		1.5×10^{13}	0.0	0.0	m	(48)
Reactions of CHCHCHO						
Decomposition by β-scission						
C ₂ H ₂ + CHO = CHCHCHO		6.0×10^{11}	0.0	7.7	n	(49)
Combination						
CHCHCHO + H = C ₂ H ₃ CHO		1.0×10^{14}	0.0	0.0	b	(50)
SECONDARY MECHANISM						
Reactions of FA (CH ₂ CCHCHO)						
Decompositions						
FA = C ₃ H ₃ + CHO	(P = 4.7 kPa)	3.6×10^{14}	0.0	69.88	o	(51)
	(P → ∞)	7.9×10^{14}	0.0	69.88	o	(51')
FA = pC ₃ H ₄ + CO	(P = 4.7 kPa)	8.0×10^{62}	-15.352	64.415	a	(52)
	(P → ∞)	6.8×10^{11}	0.419	44.231	a	(52')
Reactions of methylfuran and derived radicals						
Unimolecular initiations						
Methylfuran = C ₄ H ₆ -2 + CO		2.3×10^{15}	0.0	85.1	f	(53)
Methylfuran = 1,3-C ₄ H ₆ + CO		3.5×10^{15}	0.0	79.5	f	(54)
Methylfuran = 1,2-C ₄ H ₆ + CO		4.5×10^{15}	0.0	85.1	f	(55)
Methylfuran = C ₄ H ₆ -1 + CO		2.8×10^{15}	0.0	79.5	f	(56)
Methylfuran = pC ₃ H ₄ + CH ₂ CO		5.8×10^{15}	0.0	82.9	f	(57)
Methylfuran = C ₂ H ₂ + C ₂ H ₄ + CO		1.7×10^{15}	0.0	79.5	f	(58)
Methylfuran = C ₃ H ₃ + CH ₃ CO		4.0×10^{16}	0.0	90.5	f	(59)
Methylfuran = nC ₄ H ₅ + CHO		4.0×10^{16}	0.0	106.0	f	(60)
Bimolecular initiation						
Methylfuran + O ₂ = furylCH ₂ + HO ₂		2.2×10^7	2.5	46.045	p	(61)
Metatheses						
Methylfuran + H = furylCH ₂ + H ₂		3.0×10^{14}	0.0	9.0	f	(62)
Methylfuran + O = furylCH ₂ + OH		6.0×10^{10}	0.7	7.632	q	(63)
Methylfuran + OH = furylCH ₂ + H ₂ O		6.5×10^6	2.0	0.447	r	(64)
Methylfuran + HO ₂ = furylCH ₂ + H ₂ O ₂		7.0×10^2	3.0	12.0	s	(65)
Methylfuran + CH ₃ = furylCH ₂ + CH ₄		1.5×10^{12}	0.0	10.0	f	(66)
Methylfuran + C ₂ H ₃ = furylCH ₂ + C ₂ H ₄		2.2×10^0	3.5	4.68	s	(67)
Methylfuran + C ₃ H ₃ = furylCH ₂ + pC ₃ H ₄		8.0×10^{11}	0.0	10.0	f	(68)
Methylfuran + C ₃ H ₅ = furylCH ₂ + C ₃ H ₆		8.0×10^{11}	0.0	12.0	f	(69)
Methylfuran + iC ₄ H ₃ = furylCH ₂ + C ₄ H ₄		8.0×10^{11}	0.0	8.0	f	(70)
Combinations						
Methylfuran = furylCH ₂ + H		1.6×10^{16}	0.0	86.0	f	(71)
Decompositions and oxidation of the obtained radicals						
FurylCH ₂ = nC ₄ H ₅ + CO		2.3×10^{15}	0.0	71.0	f	(72)
FurylCH ₂ = C ₃ H ₃ + CH ₂ CO		2.3×10^{15}	0.0	64.0	f	(73)
FurylCH ₂ = C ₄ H ₄ + CHO		2.3×10^{15}	0.0	64.0	f	(74)
FurylCH ₂ = C ₂ H ₂ + C ₂ H ₃ + CO		3.3×10^{15}	0.0	76.7	f	(75)
FurylCH ₂ + O ₂ = furylCH ₂ O + O		6.3×10^{12}	0.0	40.0	t	(76)
FurylCH ₂ + O = furyl-2 + HCHO		1.6×10^{14}	0.0	0.0	t	(77)
FurylCH ₂ O = furyl-2 + HCHO		2.0×10^{13}	0.0	27.5	u	(78)
Reactions of but-3-ynal (C ₄ H ₄ O)						
H-abstractions						
CHCCH ₂ CHO + H = C ₃ H ₃ + H ₂ + CO		4.0×10^{13}	0.0	4.2	v	(79)

$\text{CHCCH}_2\text{CHO} + \text{OH} = \text{C}_3\text{H}_3 + \text{H}_2\text{O} + \text{CO}$	4.2×10^{12}	0.0	0.5	w	(80)
$\text{CHCCH}_2\text{CHO} + \text{CH}_3 = \text{C}_3\text{H}_3 + \text{CH}_4 + \text{CO}$	2.0×10^{-6}	5.6	2.5	x	(81)
Reactions of 3-butenal ($\text{C}_4\text{H}_6\text{O}$)					
H-abstractions					
$\text{CH}_2\text{CHCH}_2\text{CHO} + \text{H} = \text{C}_3\text{H}_5 + \text{H}_2 + \text{CO}$	4.0×10^{13}	0.0	4.2	v	(82)
$\text{CH}_2\text{CHCH}_2\text{CHO} + \text{OH} = \text{C}_3\text{H}_5 + \text{H}_2\text{O} + \text{CO}$	4.2×10^{12}	0.0	0.5	w	(83)
$\text{CH}_2\text{CHCH}_2\text{CHO} + \text{CH}_3 = \text{C}_3\text{H}_5 + \text{CH}_4 + \text{CO}$	2.0×10^{-6}	5.6	2.5	x	(84)
Reactions of 2-methyl-but-3-ynal ($\text{C}_5\text{H}_6\text{O}$)					
H-abstractions					
$\text{C}_5\text{H}_6\text{O} + \text{H} = \text{C}_4\text{H}_5\text{-1s} + \text{H}_2 + \text{CO}$	4.0×10^{13}	0.0	4.2	v	(85)
$\text{C}_5\text{H}_6\text{O} + \text{OH} = \text{C}_4\text{H}_5\text{-1s} + \text{H}_2\text{O} + \text{CO}$	4.2×10^{12}	0.0	0.5	w	(86)
$\text{C}_5\text{H}_6\text{O} + \text{CH}_3 = \text{C}_4\text{H}_5\text{-1s} + \text{CH}_4 + \text{CO}$	2.0×10^{-6}	5.6	2.5	x	(87)
Reactions of 2-methyl-3-butenal ($\text{C}_5\text{H}_8\text{O}$)					
H-abstractions					
$\text{C}_5\text{H}_8\text{O} + \text{H} = \text{nC}_4\text{H}_7 + \text{H}_2 + \text{CO}$	4.0×10^{13}	0.0	4.2	v	(88)
$\text{C}_5\text{H}_8\text{O} + \text{OH} = \text{nC}_4\text{H}_7 + \text{H}_2\text{O} + \text{CO}$	4.2×10^{12}	0.0	0.5	w	(89)
$\text{C}_5\text{H}_8\text{O} + \text{CH}_3 = \text{nC}_4\text{H}_7 + \text{CH}_4 + \text{CO}$	2.0×10^{-6}	5.6	2.5	x	(90)
Reactions of dihydrofuran ($\text{C}_4\text{H}_6\text{O}$) and derived radicals					
Bimolecular initiation					
$\text{Furan23H} + \text{O}_2 = \text{C}_4\text{H}_5\text{O-2} + \text{HO}_2$	1.4×10^{13}	0.0	47.6	c	(91)
$\text{furan23H} + \text{O}_2 = \text{C}_4\text{H}_5\text{O-3} + \text{HO}_2$	1.4×10^{12}	0.0	35.6	c	(92)
$\text{furan25H} + \text{O}_2 = \text{C}_4\text{H}_5\text{O-3} + \text{HO}_2$	2.8×10^{12}	0.0	35.6	c	(93)
Metatheses					
$\text{Furan23H} + \text{H} = \text{C}_4\text{H}_5\text{O-2} + \text{H}_2$	9.0×10^6	2.0	5.0	e	(94)
$\text{Furan23H} + \text{H} = \text{C}_4\text{H}_5\text{O-3} + \text{H}_2$	5.4×10^4	2.5	-1.9	e	(95)
$\text{Furan25H} + \text{H} = \text{C}_4\text{H}_5\text{O-3} + \text{H}_2$	1.1×10^5	2.5	-1.9	e	(96)
$\text{Furan23H} + \text{O} = \text{C}_4\text{H}_5\text{O-2} + \text{OH}$	2.6×10^{13}	0.0	5.2	e	(97)
$\text{Furan23H} + \text{O} = \text{C}_4\text{H}_5\text{O-3} + \text{OH}$	8.8×10^{10}	0.7	3.25	e	(98)
$\text{Furan25H} + \text{O} = \text{C}_4\text{H}_5\text{O-2} + \text{OH}$	1.8×10^{11}	0.7	3.25	e	(99)
$\text{Furan23H} + \text{OH} = \text{C}_4\text{H}_5\text{O-2} + \text{H}_2\text{O}$	2.6×10^6	2.0	-0.77	e	(100)
$\text{Furan23H} + \text{OH} = \text{C}_4\text{H}_5\text{O-3} + \text{H}_2\text{O}$	3.0×10^6	2.0	-1.52	e	(101)
$\text{Furan25H} + \text{OH} = \text{C}_4\text{H}_5\text{O-3} + \text{H}_2\text{O}$	6.0×10^6	2.0	-1.52	e	(102)
$\text{Furan23H} + \text{HO}_2 = \text{C}_4\text{H}_5\text{O-2} + \text{H}_2\text{O}_2$	4.0×10^{11}	0.0	15.5	e	(103)
$\text{Furan23H} + \text{HO}_2 = \text{C}_4\text{H}_5\text{O-3} + \text{H}_2\text{O}_2$	6.4×10^3	2.6	12.4	e	(104)
$\text{Furan25H} + \text{HO}_2 = \text{C}_4\text{H}_5\text{O-3} + \text{H}_2\text{O}_2$	1.3×10^4	2.6	12.4	e	(105)
$\text{Furan23H} + \text{CH}_3 = \text{C}_4\text{H}_5\text{O-2} + \text{CH}_4$	2.0×10^{11}	0.0	9.6	e	(106)
$\text{Furan23H} + \text{CH}_3 = \text{C}_4\text{H}_5\text{O-3} + \text{CH}_4$	1.0×10^{11}	0.0	7.3	e	(107)
$\text{Furan25H} + \text{CH}_3 = \text{C}_4\text{H}_5\text{O-3} + \text{CH}_4$	2.0×10^{11}	0.0	7.3	e	(108)
Additions and decompositions					
$\text{Furan23H} + \text{H} = \text{THF-2yl}$	1.0×10^{14}	0.0	3.26	e	(109)
$\text{Furan23H} + \text{H} = \text{THF-3yl}$	1.0×10^{14}	0.0	3.26	e	(110)
$\text{Furan25H} + \text{H} = \text{THF-3yl}$	1.0×10^{14}	0.0	3.26	e	(111)
$\text{Furan23H} + \text{OH} \Rightarrow \text{HCHO} + \text{C}_2\text{H}_4 + \text{CHO}$	2.7×10^{12}	0.0	-1.1	e	(112)
$\text{Furan25H} + \text{OH} \Rightarrow \text{HCHO} + \text{C}_2\text{H}_4 + \text{CHO}$	2.7×10^{12}	0.0	-1.1	e	(113)
Decompositions and combinations of the obtained radicals					
$\text{THF-2yl} = \text{C}_2\text{H}_4 + \text{CH}_2\text{CHO}$	2.0×10^{14}	0.005	35.6	y	(114)
$\text{THF-3yl} = \text{HCHO} + \text{C}_3\text{H}_5$	2.0×10^{14}	0.005	35.6	y	(115)
$\text{THF-2yl} + \text{H} = \text{THF}$	1.0×10^{14}	0.0	0.0	b	(116)
$\text{THF-3yl} + \text{H} = \text{THF}$	1.0×10^{14}	0.0	0.0	b	(117)
Reactions of THF ($\text{C}_4\text{H}_8\text{O}$)					
Bimolecular initiation					
$\text{THF} + \text{O}_2 = \text{THF-2yl} + \text{HO}_2$	2.8×10^{13}	0.0	47.6	c	(118)
$\text{THF} + \text{O}_2 = \text{THF-3yl} + \text{HO}_2$	2.8×10^{13}	0.0	47.6	c	(119)
Metatheses					
$\text{THF} + \text{H} = \text{THF-2yl} + \text{H}_2$	1.8×10^7	2.0	5.0	e	(120)
$\text{THF} + \text{H} = \text{THF-3yl} + \text{H}_2$	1.8×10^7	2.0	5.0	e	(121)
$\text{THF} + \text{O} = \text{THF-2yl} + \text{OH}$	5.2×10^{13}	0.0	5.2	e	(122)
$\text{THF} + \text{O} = \text{THF-3yl} + \text{OH}$	5.2×10^{13}	0.0	5.2	e	(123)
$\text{THF} + \text{OH} = \text{THF-2yl} + \text{H}_2\text{O}$	5.2×10^6	2.0	-0.77	e	(124)
$\text{THF} + \text{OH} = \text{THF-3yl} + \text{H}_2\text{O}$	5.2×10^6	2.0	-0.77	e	(125)
$\text{THF} + \text{HO}_2 = \text{THF-2yl} + \text{H}_2\text{O}_2$	8.0×10^{11}	0.0	15.5	e	(126)

THF + HO ₂ = THF-3yl + H ₂ O ₂	8.0 × 10 ¹¹	0.0	15.5	e	(127)
THF + CH ₃ = THF-2yl + CH ₄	4.0 × 10 ¹¹	0.0	9.6	e	(128)
THF + CH ₃ = THF-3yl + CH ₄	4.0 × 10 ¹¹	0.0	9.6	e	(129)

Note: the rate constants are given in the form $k = A T^n \exp(-E_a/RT)$ where A has units of cm, mol and s, T has units of K, and E_a has units of kcal/mol.

^a Rate constant calculated in this work.

^b Rate constant taken equal to that of the recombination of H atoms with alkyl radicals as proposed by Allara and Shaw [36].

^c Rate constant calculated as proposed by Ingham et al. [37], but E_a corrected with enthalpies of the bimolecular reaction.

^d Rate constant estimated by analogy with the values proposed by Gueniche et al. [38] for the similar reaction of 1,3-butadiene.

^e Rate constant estimated by using the correlations proposed by Heyberger et al. [39] in the case of alkenes.

^f Rate constant taken equal to the values proposed by Lifshitz et al. [40] for methylfuran.

^g Rate constant taken equal to that of the isomerization of *i*C₄H₅ and *n*C₄H₅ radicals as proposed by Leung and Lindstedt [41].

^h Rate constant estimated by analogy with values proposed by Mebel et al. [42] for reactions of O₂ + C₂H₃.

ⁱ Rate constant estimated by analogy with values proposed by Dagaut et al. [43] for reactions of O + C₂H₃.

^j Rate constant taken equal to the values proposed by Gueniche et al. [38] for the similar reaction of IC₄H₇-1 and IC₄H₇Y.

^k Rate constant estimated by using the correlations proposed by Touchard et al. [44] in the case of low temperature oxidation of 1-pentene.

^l Rate constant estimated by analogy with values proposed by Baulch et al. [45] for the similar reaction of O + C₂H₅.

^m Rate constant calculated using the modified collision theory at 1200 K using software KINGAS [56].

ⁿ Rate constant estimated by analogy with values proposed by Baulch et al. [45] for reaction of C₂H₂ + CH₃ = sC₃H₅.

^o Rate constant taken equal to the values proposed by Sendt et al. [21] for formyl allene, with the A-factor divided by 2.2 for flame conditions.

^p Rate constant estimated by analogy with values proposed by Oehlschlaeger et al. [46] for reaction of toluene + O₂.

^q Rate constant estimated by analogy with values proposed by Pitz et al. [47] for reaction of toluene + O.

^r Rate constant estimated by analogy with values proposed by Knispel et al. [48] for reaction of toluene + OH.

^s Rate constant estimated by analogy with values proposed by Mehl et al. [49] for reaction of toluene + HO₂.

^t Rate constant estimated by using the correlations proposed by Brezinsky et al. [57] in the case of benzyl radical.

^u Rate constant estimated by analogy with values proposed by Bounaceur et al. [58] for reaction of C₆H₅CH₂O.




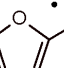
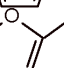
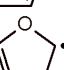
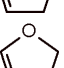
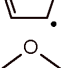
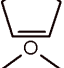
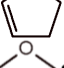
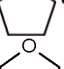

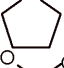
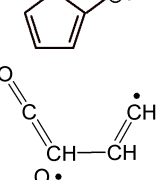
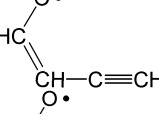
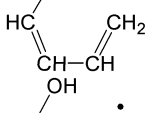
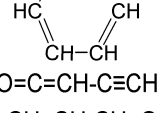
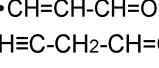
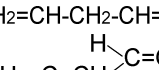
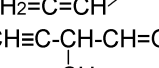
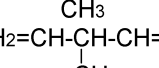
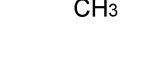


^v Rate constant estimated by analogy with values proposed by Warnatz [50] for the similar reaction of CH₃CHO + H.

^w Rate constant estimated by analogy with values proposed by Cavanagh et al. [51] for the similar reaction of CH₃CHO + OH.

^x Rate constant estimated by analogy with values proposed by Baulch et al. [45] for the similar reaction of CH₃CHO + CH₃.

^y Rate constant estimated by analogy with values proposed by Sirjean et al. [52] for the ring opening reaction of C₅H₉#.

Table 3 Thermochemical data of furan and its derived species.

Species	Structure	$\Delta_f H_{298K}^\circ$ (kcal/mol)	S_{298K}° (cal/mol/K)	C_p° (T) (cal/mol/K)							
				298	400	500	600	800	1000	1500	2000
Furan*		-8.23	65.2	15.5	21.1	25.6	29.2	34.3	37.7	42.7	45.4
Furyl-2*		59.0	66.5	15.1	20.1	23.9	27.0	31.3	34.2	38.2	40.3
Furyl-3*		59.2	66.3	15.0	19.9	23.8	26.9	31.2	34.1	38.1	40.3
Methylfuran*		-18.9	73.8	21.2	27.8	33.3	37.9	44.8	49.6	56.6	60.5
FurylCH ₂ *		14.4	72.6	21.3	28.0	33.3	37.4	43.3	47.3	53.2	56.4
C ₄ H ₅ O-2		18.1	68.2	21.4	26.1	30.2	33.7	39.1	42.7	43.7	44.7
C ₄ H ₅ O-3		8.45	68.1	21.2	25.8	29.9	33.4	38.9	42.5	43.6	44.7
Furan25H		-14.18	65.1	15.9	23.0	28.9	33.6	40.7	45.7	57.3	61.4
Furan23H		-21.76	67.0	21.7	27.0	31.6	35.7	42.0	46.2	48.2	50.0
THF-2yl		-4.09	71.9	24.9	31.1	36.2	40.6	47.2	51.3	53.2	55.0
THF-3yl		-1.59	71.9	24.9	31.1	36.3	40.6	47.2	51.3	53.2	55.0
THF		-44.08	69.3	25.2	32.0	37.7	42.6	50.0	54.8	57.7	60.2
FurylCH ₂ O		0.25	82.4	26.4	33.4	38.8	43.0	48.8	53.0	67.3	72.7
CHCHCHCO*		66.4	74.5	19.7	23.5	26.4	28.7	32.2	34.7	38.4	40.5
CHCCHCHO		67.0	82.8	19.0	22.3	25.1	27.4	30.9	33.3	37.3	40.3
CH ₂ CHCHCHO		23.9	83.1	20.7	25.1	28.8	31.9	36.7	40.0	45.8	50.1
CHCHCHCHOH		49.3	84.7	22.0	26.3	29.7	32.6	37.1	40.3	45.8	49.9
CHCCHCO*		47.1	70.9	18.9	21.9	24.2	25.9	28.6	30.5	33.5	35.1
CHCHCHO		42.4	72.4	13.9	17.5	20.6	23.4	28.3	32.3	36.7	39.5
CHCCH ₂ CHO		18.7	76.3	20.9	24.4	27.4	30.2	34.5	37.3	38.8	40.7
CH ₂ CHCH ₂ CHO		-18.9	80.4	22.0	26.7	30.9	34.5	40.4	44.3	46.3	49.0
CH ₂ CCHCHO (FA)*		15.6	73.4	19.7	24.0	27.6	30.6	35.2	38.5	43.1	45.5
C ₅ H ₆ O		14.8	83.3	25.8	31.0	35.5	39.4	45.6	49.5	51.4	53.9
C ₅ H ₈ O		-24.5	86.9	26.9	33.3	38.9	43.8	51.5	56.5	58.9	62.2

Note: Thermochemical data have been calculated by software THERGAS [31], except for species marked with* for which they have been obtained from theoretical calculation (see text).

Table 4 Flame species measured with their respective IEs, maximum mole fractions (X_{\max}), and positions (P, mm) in furan/oxygen/argon flames

m/e	Formula	Species	IEs		Mole Fractions					
			Literature ^a	This Work ^b	$\Phi = 1.4$		$\Phi = 1.8$		$\Phi = 2.2$	
					P	X_{\max}	P	X_{\max}	P	X_{\max}
15	CH ₃	methyl radical	9.84	9.79	3.5	8.9E-04	5.5	9.8E-04	8.5	8.9E-04
16	CH ₄	methane	12.71	12.71	3.5	2.1E-03	5.0	3.9E-03	8.0	4.3E-03
26	C ₂ H ₂	acetylene	11.40	11.35	3.5	1.6E-02	5.5	2.8E-02	8.5	3.9E-02
28	C ₂ H ₄	ethylene	10.52	10.49	3.5	5.8E-03	4.5	7.1E-03	7.5	7.7E-03
30	CH ₂ O	formaldehyde	10.88	10.84	3.0	3.1E-03	4.0	3.3E-03	6.5	3.4E-03
32	CH ₃ OH	methyl alcohol	10.84	10.83	-	-	-	-	-	-
39	C ₃ H ₃	propargyl radical	8.67	8.67	3.5	6.1E-04	5.5	1.1E-03	8.5	1.5E-03
40	aC ₃ H ₄	allene	9.83	9.83	3.5	3.6E-04	5.0	5.3E-04	8.0	8.1E-04
	pC ₃ H ₄	propyne	10.36	10.34	3.0	7.7E-04	5.0	2.4E-03	8.0	4.2E-03
41	C ₃ H ₅	allyl radical	8.18	8.19	3.0	2.4E-04	5.0	2.6E-04	8.0	1.3E-04
42	CH ₂ CO	ketene	9.62	9.58	2.5	1.4E-03	5.0	1.8E-03	7.0	2.3E-03
44 ^c	C ₂ H ₄ O	ethenol	9.33	9.30	3.0	4.2E-05	4.0	4.7E-05	6.0	4.8E-05
	C ₂ H ₄ O	acetaldehyde	10.23	10.22						
50	C ₄ H ₂	diacetylene	10.17	10.14	4.0	1.6E-04	5.0	6.7E-04	6.0	7.3E-04
51	C ₄ H ₃	CH ₂ CCCH	8.06	8.10	-	-	-	-	-	-
52 ^c	C ₄ H ₄	1,2,3-butatriene	9.15	9.15	3.5	5.8E-04	5.5	7.4E-04	8.5	1.2E-03
	C ₄ H ₄	vinylacetylene	9.58	9.56						
54	C ₄ H ₆	1,3-butadiene	9.07	9.04	3.0	1.3E-04	4.5	1.8E-04	8.0	2.6E-04
55	C ₃ H ₃ O	HC=CH-CHO		9.54						
56 ^c	C ₃ H ₄ O	methylketene	8.95	8.91	2.0	1.9E-04	3.5	2.6E-03	6.0	2.9E-03
	C ₃ H ₄ O	propenal	10.11	10.09						
58	C ₃ H ₆ O	acetone	9.70	9.70	-	-	-	-	-	-
64 ^c	C ₅ H ₄	1,2,3,4-pentatetraene	8.67	8.72	2.5	1.2E-05	5.5	2.5E-05	8.0	6.9E-05
	C ₅ H ₄	1,3-pentadiyne	9.50	9.48						
65	C ₅ H ₅	cyclopentadienyl radical	8.41	8.41	2.5	1.6E-05	5.5	3.4E-05	8.5	5.8E-05
66 ^c	C ₅ H ₆	1,3-cyclopentadiene	8.57	8.54	2.5	2.3E-05	4.5	3.6E-05	8.0	4.6E-05
	C ₄ H ₂ O	ethynylketene	8.77±0.15 ^d	8.70						
68	C ₄ H ₄ O	furan	8.88	8.86				fuel		
74	C ₆ H ₂	1,3,5-hexatriyne	9.50	9.48	2.5	3.3E-05	6.5	4.0E-05	9.0	5.5E-05
76	C ₆ H ₄	benzyne	9.07	9.06	3.0	1.6E-05	2.5	2.2E-05	8.5	3.9E-05
		3-hexene-1,5-diyne	9.03							
78 ^c	C ₆ H ₆	fulvene	8.36	8.40	3.5	6.0E-05	5.0	8.6E-05	8.0	1.5E-04
	C ₆ H ₆	benzene	9.26	9.23						
80	C ₆ H ₈	1,3-cyclohexadiene	8.25	8.23	2.5	2.0E-05	4.0	3.0E-05	4.5	4.0E-05
82	C ₅ H ₆ O	2-methyl-furan	8.38	8.36	2.0	1.6E-05	4.0	2.3E-05	7.0	3.8E-05
84	C ₅ H ₈ O	4-pentyn-2-ol	10.24	10.21	-	-	-	-	-	-
92	C ₇ H ₈	toluene	8.83	8.80	3.5	1.0E-06	4.0	1.5E-06	7.0	3.4E-06
94	C ₆ H ₆ O	phenol	8.49	8.50	3.0	4.0E-06	4.5	3.1E-05	7.5	3.9E-05
102	C ₈ H ₆	phenylacetylene	8.82	8.79	—	—	—	—	8.5	2.3E-06
104	C ₈ H ₈	styrene	8.46	8.47	—	—	—	—	7.0	4.9E-06

Note: ^a Refers to [59]; ^b errors for stable species are ±0.05eV, for radicals are ±0.10eV; ^c the values are the total mole fraction of a specific mass, for example, the mole fraction of mass 44 includes both ethenol and acetaldehyde; ^d refers to [60].

Figures and Figure Captions

Color figure in electronic versions only

[Figure 1]

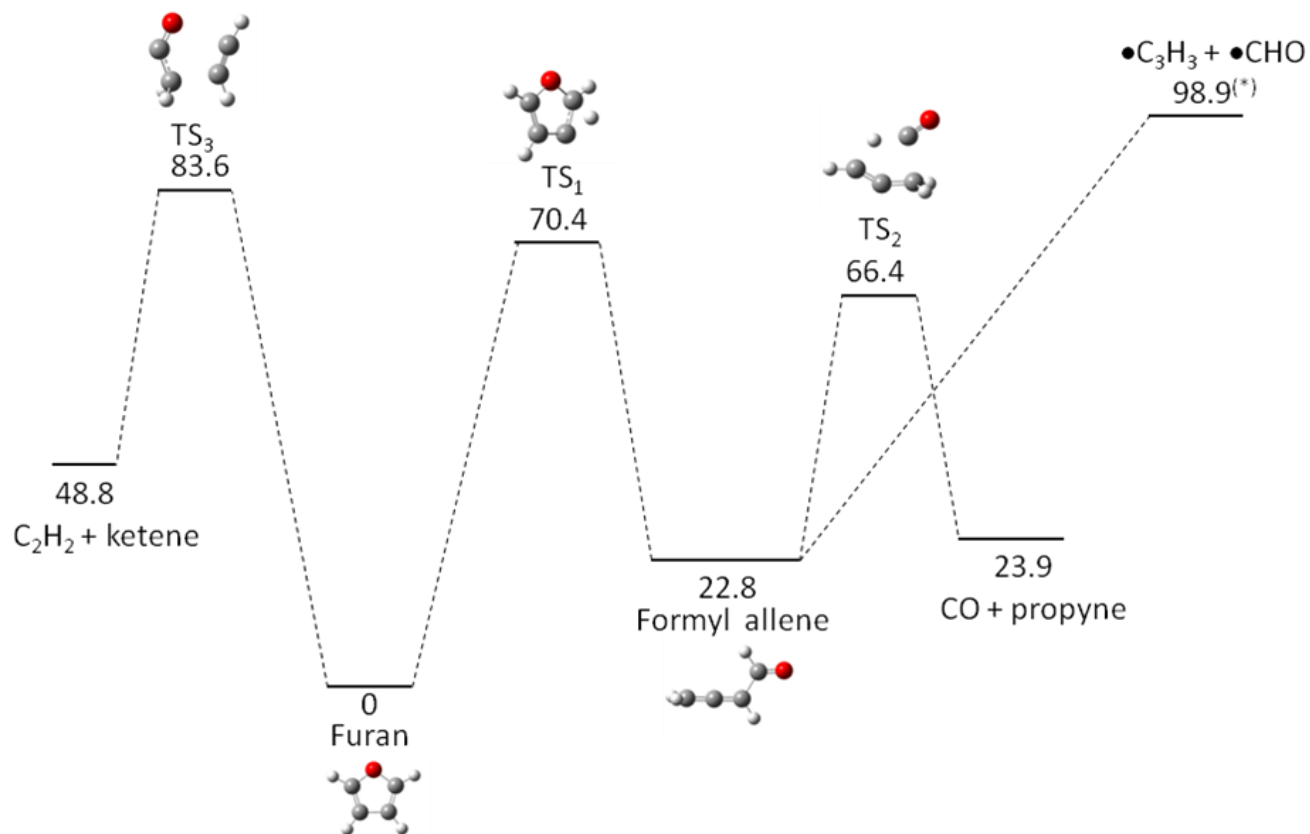


Fig. 1 Simplified potential energy surface (PES) for the unimolecular initiation of furan. The energies (in kcal mol⁻¹) are relative to furan and calculated at the CBS-QB3 level of theory at 0 K.

(*) This energy has been taken from Sendt et al. [21].

[Figure 2]

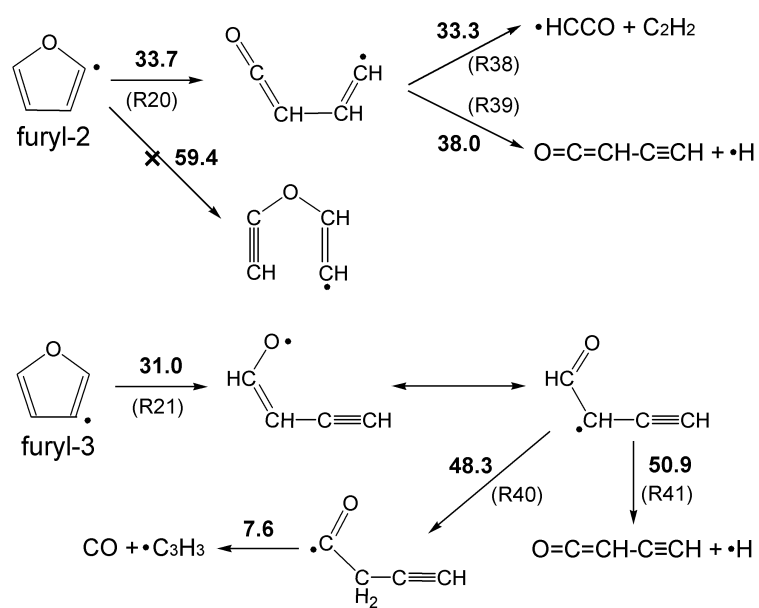


Fig. 2 Unimolecular decompositions of furyl radicals considered in this study. Activation energies (in bold) have been calculated at the CBS-QB3 level of theory, at 298 K.

[Figure 3]

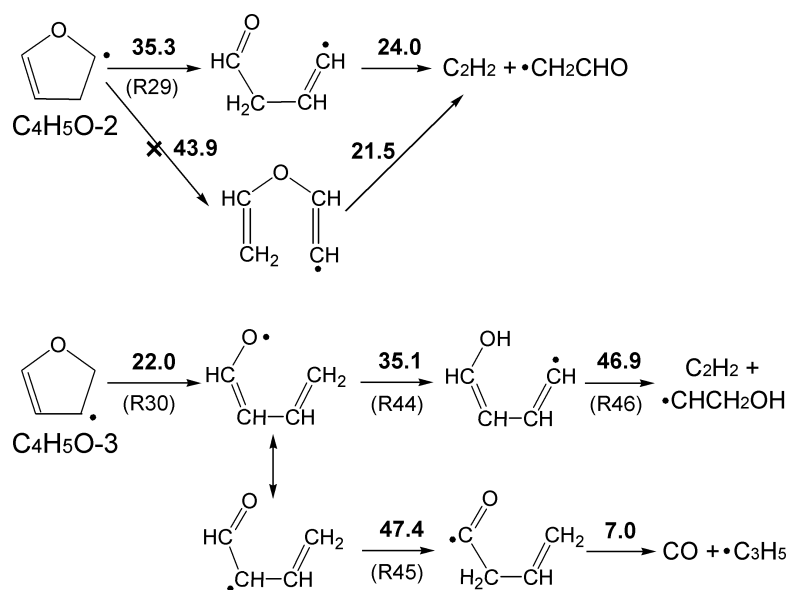


Fig. 3 Unimolecular decompositions of dihydrofuryl radicals considered in this study. Activation energies (in bold) have been calculated at the CBS-QB3 level of theory, at 298 K.

[Figure 4]

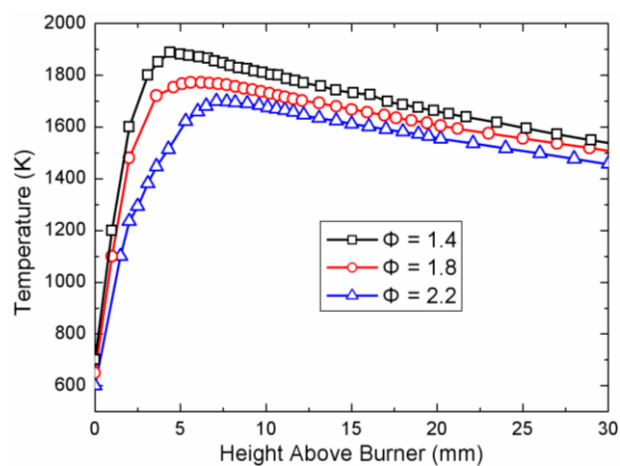


Fig. 4 Temperature profiles of the furan/O₂/Ar flames ($\Phi = 1.4, 1.8$ and 2.2).

[Figure 5]

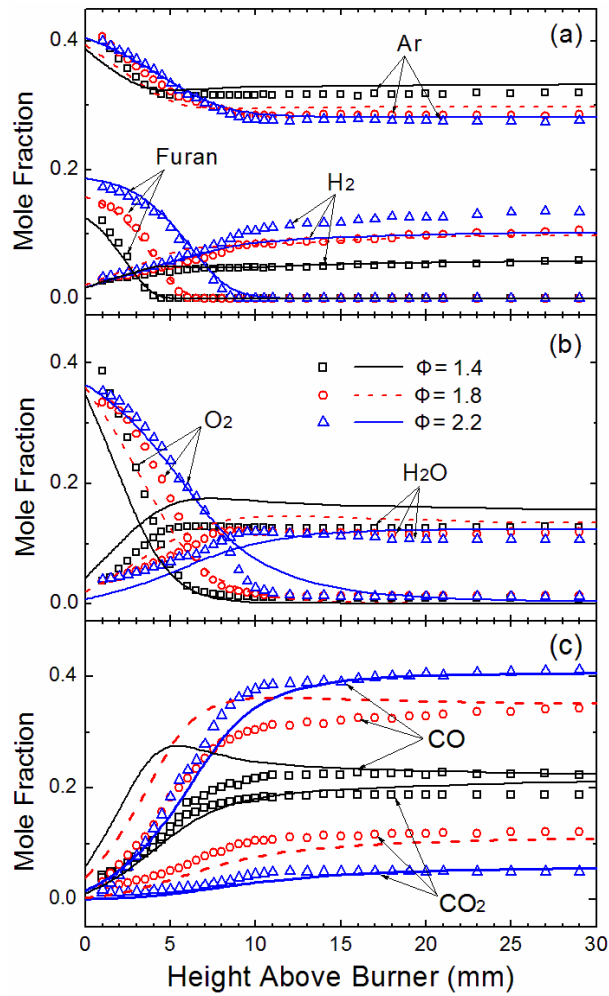


Fig. 5 Experimental (symbols) and predicted (lines) concentration profiles of Ar, O₂, furan, H₂, H₂O, CO and CO₂ in the furan/O₂/Ar flames ($\Phi = 1.4, 1.8$ and 2.2).

[Figure 6]

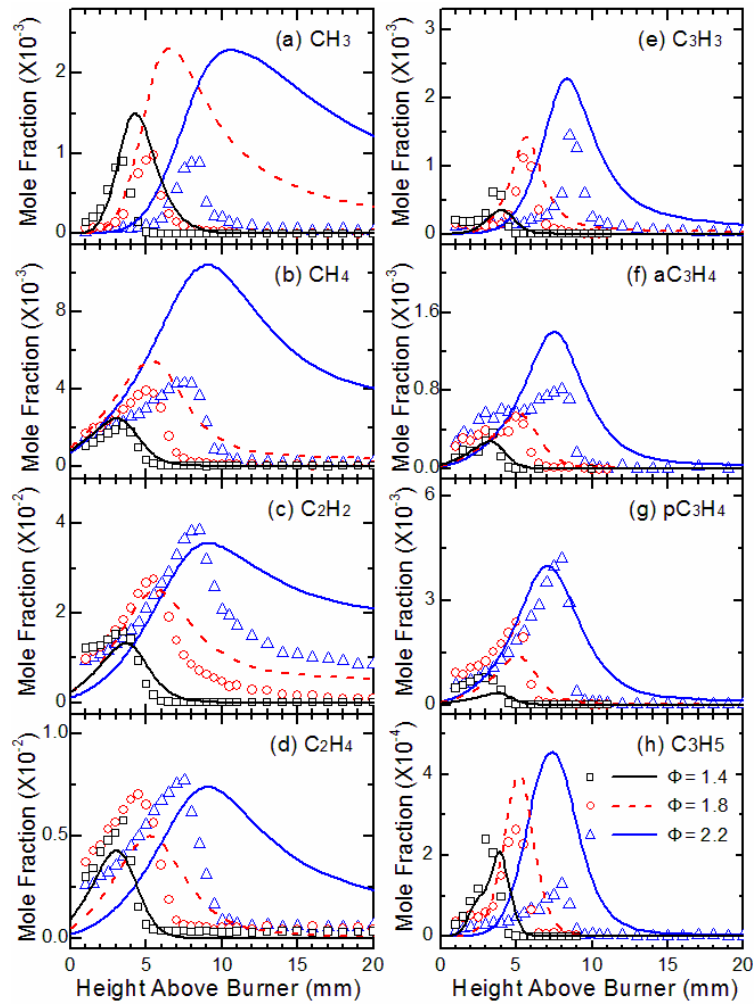


Fig. 6 Experimental (symbols) and predicted (lines) concentration profiles of (a) CH₃ (methyl radical), (b) CH₄ (methane), (c) C₂H₂ (acetylene), (d) C₂H₄ (ethylene), (e) C₃H₃ (propargyl radical), (f) aC₃H₄ (allene), (g) pC₃H₄ (propyne) and (h) C₃H₅ (allyl radical) in the furan/O₂/Ar flames ($\Phi = 1.4, 1.8$ and 2.2).

[Figure 7]

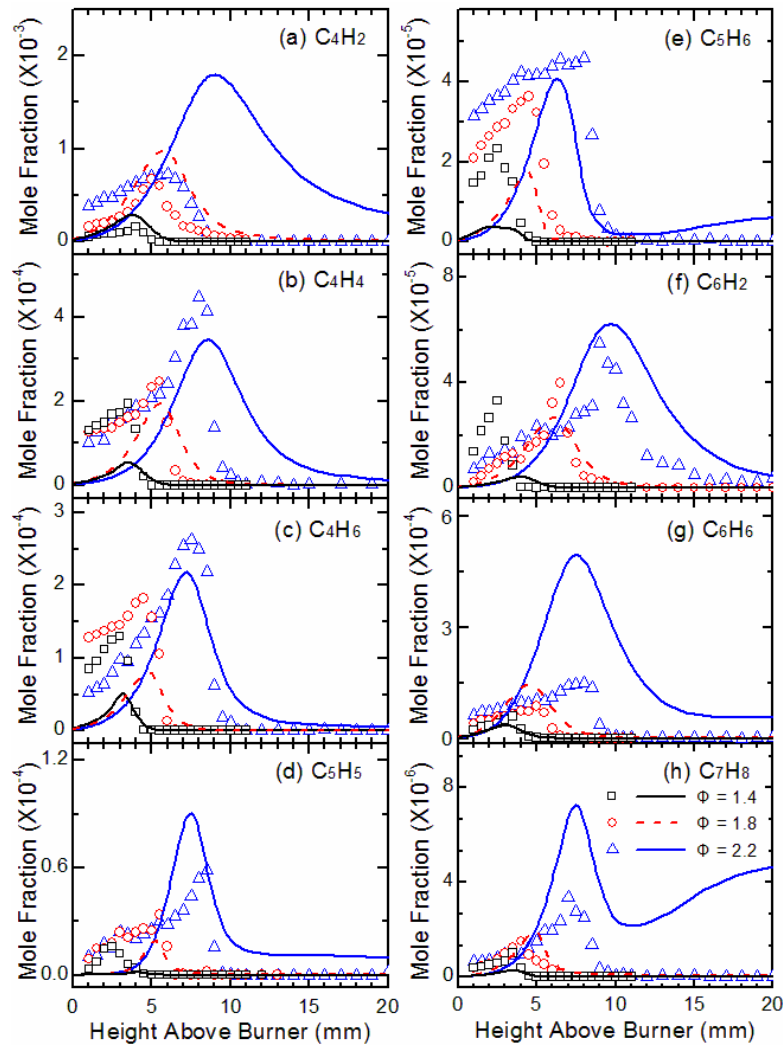


Fig. 7 Experimental (symbols) and predicted (lines) concentration profiles of (a) C_4H_2 (diacetylene), (b) C_4H_4 (vinylacetylene), (c) C_4H_6 (1,3-butadiene), (d) C_5H_5 (cyclopentadienyl radical), (e) C_5H_6 (1,3-cyclopentadiene), (f) C_6H_2 (1,3,5-hexatriyne), (g) C_6H_6 (benzene) and (h) C_7H_8 (toluene) in the furan/ O_2 /Ar flames ($\Phi = 1.4, 1.8$ and 2.2).

[Figure 8]

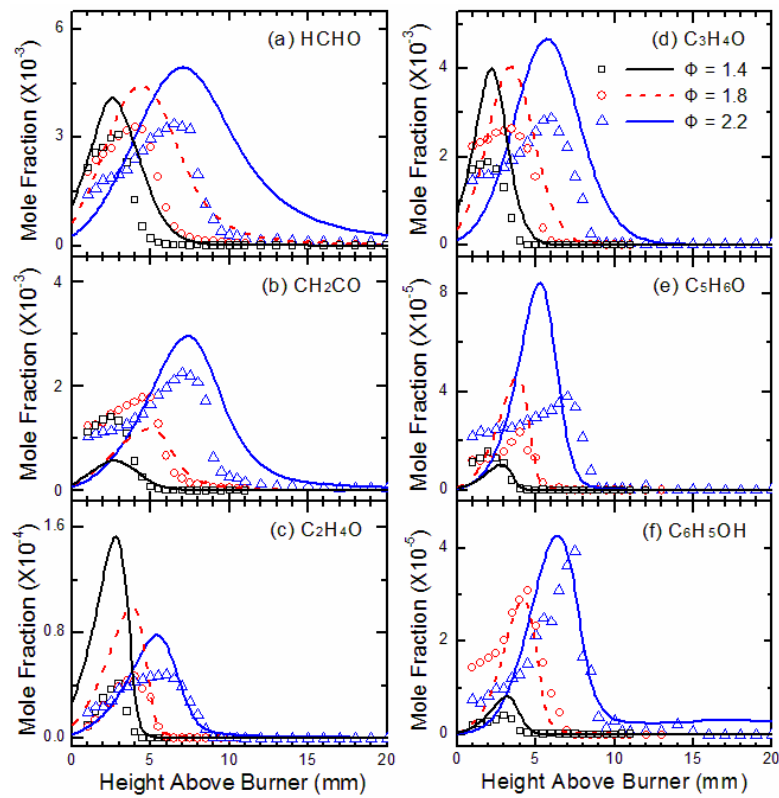


Fig. 8 Experimental (symbols) and predicted (lines) concentration profiles of (a) HCHO (formaldehyde), (b) CH₂CO (ketene), (c) C₂H₄O (acetaldehyde), (d) C₃H₄O (methylketene), (e) C₅H₆O (2-methylfuran) and (f) C₆H₅OH (phenol) in the furan/O₂/Ar flames ($\Phi = 1.4, 1.8$ and 2.2).

[Figure 9]

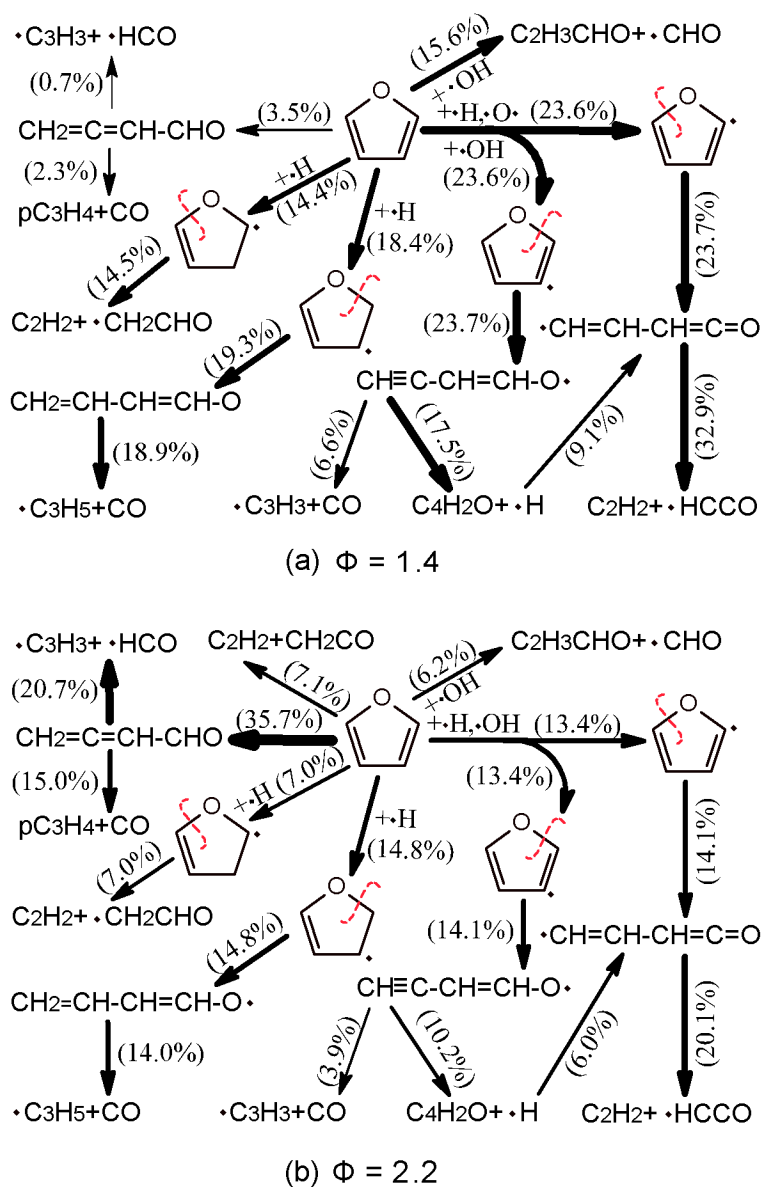


Fig. 9 Rate-of-production analysis for the consumption of furan at two equivalence ratios, (a) $\Phi = 1.4$ (flame A, at 3.7 mm from the burner, $T = 1470$ K, 88.9% furan conversion) and (b) $\Phi = 2.2$ (flame C, at 7.9 mm from the burner, $T = 1609$ K, 85.0% furan conversion).

[Figure 10]

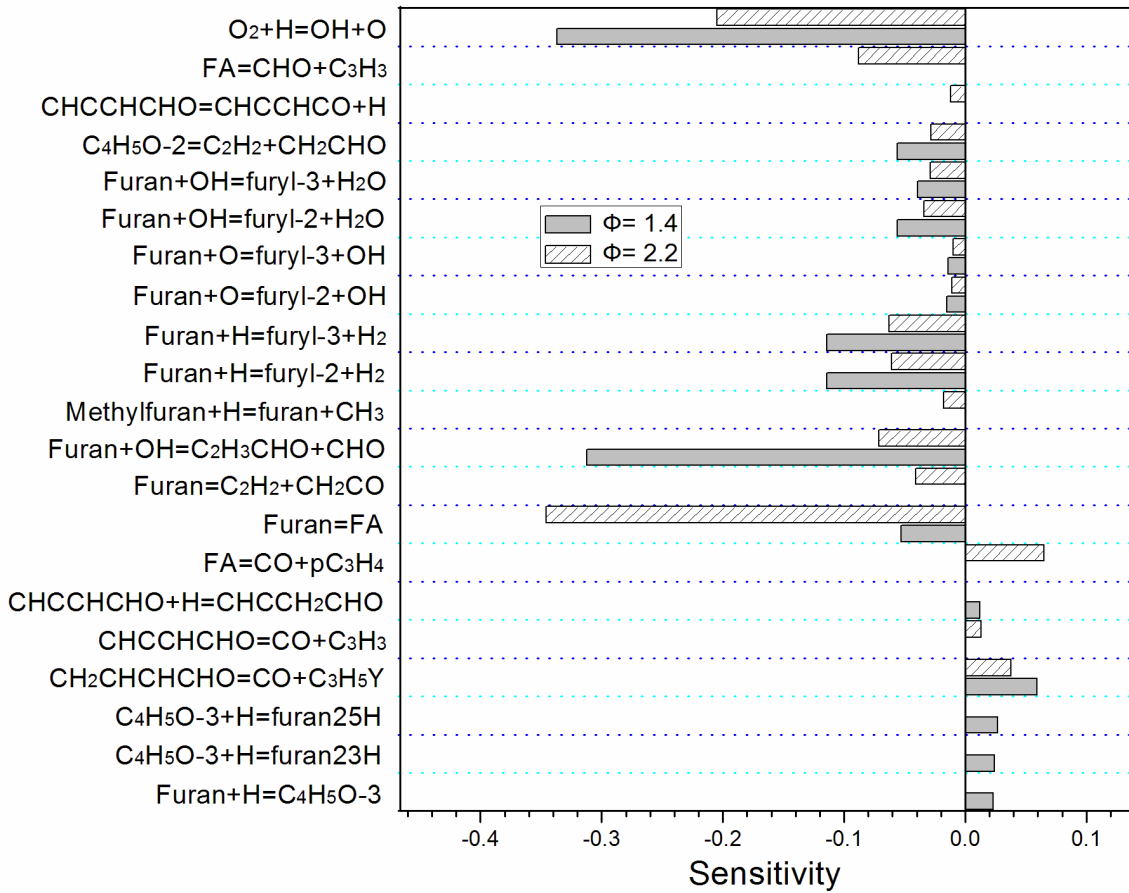


Fig. 10 Sensitivity analysis for the conversion of furan at two equivalence ratios, (a) $\Phi = 1.4$ (flame A, at 3.7 mm from the burner, $T = 1470$ K, 88.9% furan conversion) and (b) $\Phi = 2.2$ (flame C, at 7.9 mm from the burner, $T = 1609$ K, 85.0% furan conversion).

[Figure 11]

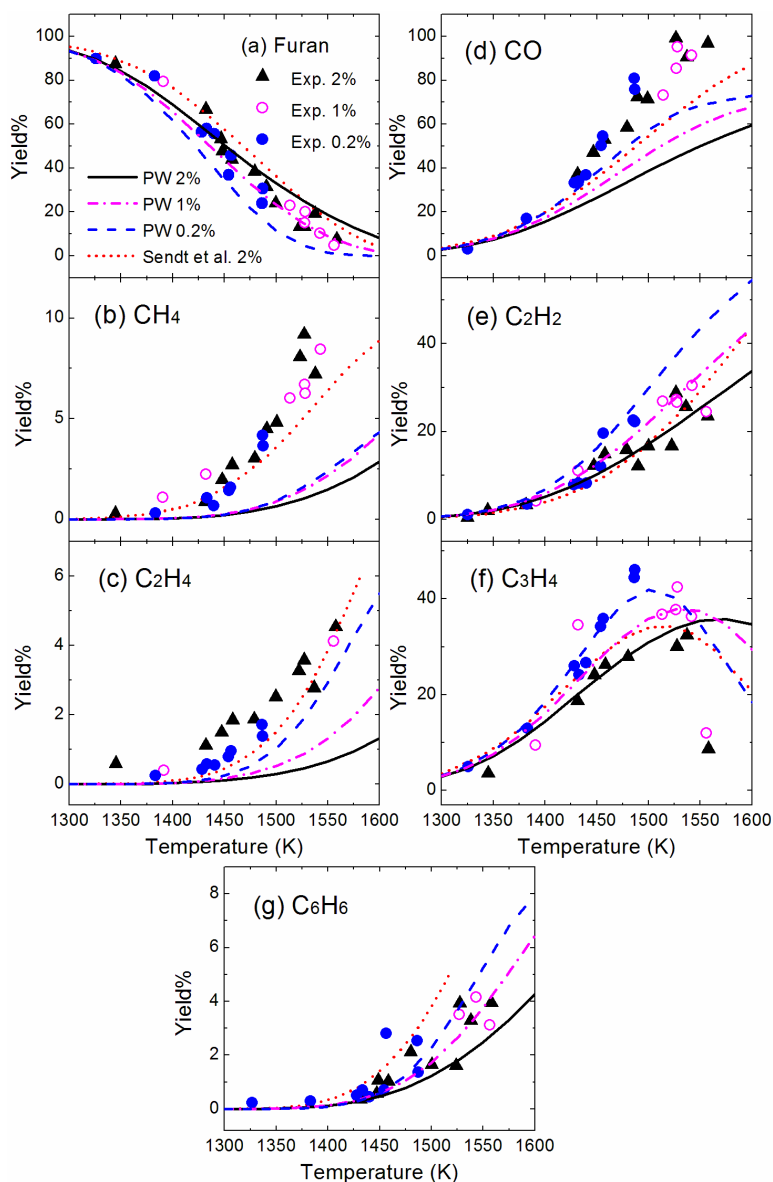


Fig. 11 Temperature dependence of designated species in the pyrolysis of furan (dilute in Ar, 20 atm): symbols are experimental results from Organ and Mackie [14]; solid (2% furan inlet), dash dot (1% furan inlet), dash lines (0.2% furan inlet) are predictions of the present work (PW) and short dash lines (2% furan inlet) are predictions by Sendt et al. [21], respectively.

[Figure 12]

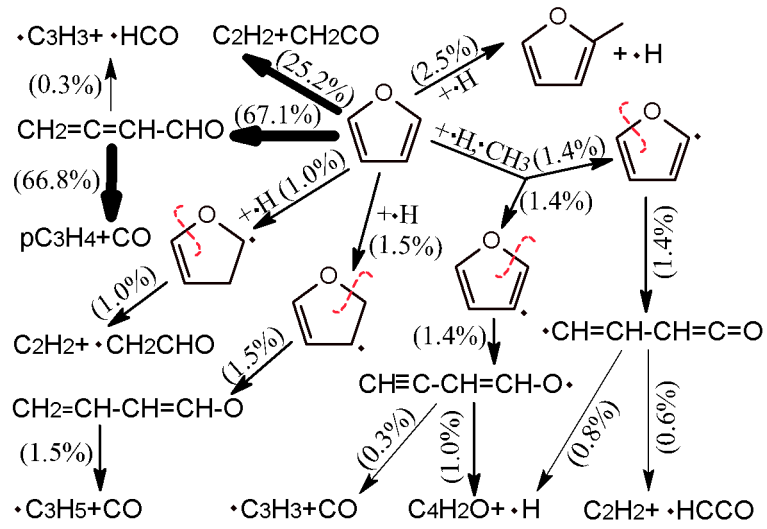


Fig. 12 Rate-of-production analysis for the consumption of furan at a temperature of 1527 K and a 64.8% conversion of furan in the furan pyrolysis.

[Figure 13]

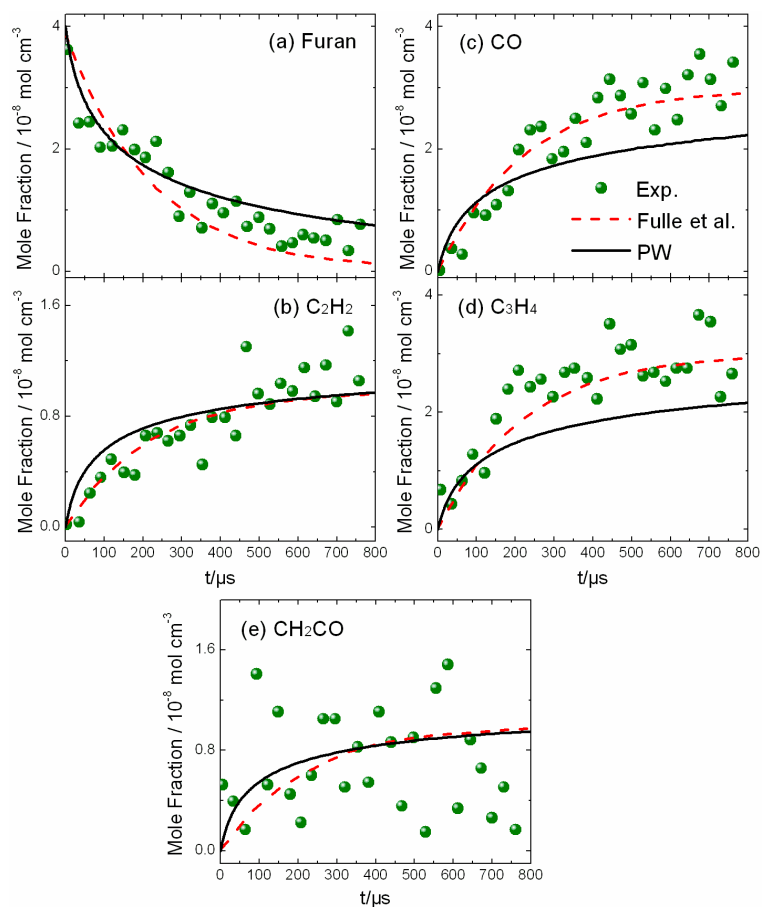


Fig. 13 Species mole fractions versus residence time during the pyrolysis of furan (2% furan/98% Ne, 1533 K, 198 Torr): symbols are experimental results from Fulle et al. [15]; solid and dashed lines are predictions of the present work (PW) and Fulle et al. [15], respectively.

[Figure 14]

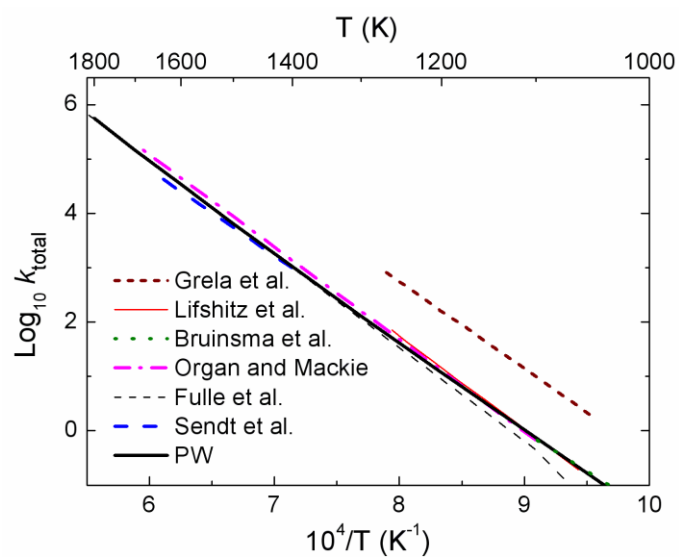


Fig. 14 Comparison of rate constants: Arrhenius plots of the rate constant for furan thermal decomposition, in which short dash line is the date of Grela et al. [11], thin solid line Lifshitz et al. [12], dot line Bruinsma et al. [13], dash dot line Organ and Mackie [14], thin dash line Fulle et al. [15], solid dash line Sendt et al. [21] and thick solid line the present work (PW).

List of Supplemental Material

A “supplemental material” is included in this paper. It consists of the following sections:

Section 1: Experimental mole fraction data of furan flames

Table S1 is the experimental mole fraction data measured in the three furan flames.

Section 2: The detailed reaction mechanism of this work

The reaction mechanism developed in this study, including 206 species and 1368 reactions, is displayed in this section.

Section 3: Isodesmic reactions

This part gives the isodesmic reactions from which the enthalpies of formation of the species listed in Table 3 are calculated.

Section 4: Geometries/Frequencies/Moments of inertia

In this section, the geometries, frequencies and moments of inertia of 34 species involved in figures 1, 2 and 3 are listed.